

REPORT DOCUMENTATION PAGE

Form Approved
OMB No. 0704-0188

Public reporting burden for this collection of information is estimated to average 1 hour per response, including the time for reviewing instructions, searching existing data sources, gathering and maintaining data needed, and completing and reviewing this collection of information. Send comments regarding this burden estimate or any other aspect of this collection of information, including suggestions for reducing this burden to Department of Defense, Washington Headquarters Services, Directorate for Information Operations and Reports (0704-0188), 1215 Jefferson Davis Highway, Suite 1204, Arlington, VA 22202-4302. Respondents should be aware that notwithstanding any other provision of law, no person shall be subject to any penalty for failing to comply with a collection of information if it does not display a current valid OMB control number. **PLEASE DO NOT RETURN YOUR FORM TO THE ABOVE ADDRESS.**

1. REPORT DATE (DD-MM-YYYY) 31-10-2002		2. REPORT TYPE FINAL		3. DATES COVERED (From - To) June 1998 to October 2002	
4. TITLE AND SUBTITLE STUDY OF PROSPECTIVE CANDIDATES FOR HIGH PERFORMANCE MAGNETS				5a. CONTRACT NUMBER N00014-98-C-0268	
				5b. GRANT NUMBER	
				5c. PROGRAM ELEMENT NUMBER	
6. AUTHOR(S) S.G. Sankar				5d. PROJECT NUMBER	
				5e. TASK NUMBER	
				5f. WORK UNIT NUMBER	
7. PERFORMING ORGANIZATION NAME(S) AND ADDRESS(ES) Advanced Materials Corporation 700 Technology Dr Pittsburgh PA 15230-2950 Carnegie Mellon University Forbes Avenue Pittsburgh PA 15213				8. PERFORMING ORGANIZATION REPORT NUMBER	
9. SPONSORING / MONITORING AGENCY NAME(S) AND ADDRESS(ES) Office of Naval Research Ballston Tower One 800 N. Quincy Street Arlington, VA 22217-5660 (Kristl Hathaway, Code 332)				10. SPONSOR/MONITOR'S ACRONYM(S)	
				11. SPONSOR/MONITOR'S REPORT NUMBER(S)	

12. DISTRIBUTION / AVAILABILITY STATEMENT UNLIMITED	
---------------------------------------------------------------	--

20021119 054

13. SUPPLEMENTARY NOTES

14. ABSTRACT The objective of this work is to examine the structural and magnetic properties of materials that are of interest in high performance magnets. (1) Fe-Pt based alloys were examined with a view to develop a process to fabricate bulk permanent magnets and to examine the effects of order-disorder phenomena on the permanent magnet properties. The co-existence of cubic and tetragonal phases gives rise to exchange-coupled spring magnets. (2) $MnBi_{1-x}R_x$ ($R = Nd, Dy$) specimens were prepared to examine the influence of R on the magnetic properties of $MnBi$. (3) $RCo_{7-x}Zr_x$ alloys stabilize in the $TbCu_7$ -type structure. Nd and Ho additions significantly modify the magnetocrystalline anisotropy behavior in these systems.

15. SUBJECT TERMS Permanent magnets, Spring magnets, Exchange coupling, FePt, MnBi, RCo7

16. SECURITY CLASSIFICATION OF:			17. LIMITATION OF ABSTRACT Unlimited	18. NUMBER OF PAGES	19a. NAME OF RESPONSIBLE PERSON S.G. Sankar
a. REPORT Unclassified	b. ABSTRACT Unclassified	c. THIS PAGE Unclassified			19b. TELEPHONE NUMBER (include area code) (412) 268 5649

STUDY OF PROSPECTIVE CANDIDATES FOR HIGH PERFORMANCE MAGNETS

Contract Number: N00014-98-C-0268

**DATA ITEM: A002
FINAL REPORT**

June 20, 1998 to October 31, 2002

Submitted by

**Advanced Materials Corporation
700 Technology Drive
P.O. Box 2950
Pittsburgh, PA 15230-2950**

Telephone: 412-268-5649

Fax: 412-268-3300

E-mail: sankar@advanced-material.com

October 2002

TABLE OF CONTENTS

ABSTRACT	3
INTRODUCTION.....	4
SIGNIFICANT RESULTS.....	4
I. Iron-Platinum Alloys.....	4
II. MnBi Alloys.....	17
III. $\text{RCo}_{7-x}\text{Zr}_x$ Systems (R=Y, Nd, Gd or Ho)	24
IV. $\text{R}_6(\text{Fe, Co})_{11}\text{M}_3$ Systems (R=rare earth, M = Ga, or Ge)	26
V. Iron Nitrides	27
SUMMARY.....	30
ACKNOWLEDGMENT.....	31
REFERENCES.....	31
PUBLICATIONS	32

Study of Prospective Candidates for High Performance Magnets

ABSTRACT

The objective of this work is to examine the structural and magnetic properties of materials that are of interest in high performance magnets. During the program, a number of alloys have been investigated.

- (1) Fe-Pt based alloys were examined with a view to develop a process to fabricate bulk permanent magnets and to examine the effects of order-disorder phenomena on the permanent magnet properties. Compositions close to $\text{Fe}_x\text{Pt}_{1-x}$ ($x = 0.5$ to 0.615) were prepared by (a) melt-extracting stoichiometric quantities of metals in an induction furnace, (b) mechanically milling the sample at ~ 77 K and (c) by melt spinning technique. Measurements of magnetic properties of these specimens show a typical saturation magnetization of 13.8 kG and 13.3 kG in the fcc and fct phases, respectively. The corresponding coercivities are 262 Oe and 3600 Oe.

FePt alloys exhibit order-disorder phenomenon. The ordered phase crystallizes in the tetragonal structure and is magnetically hard, while the disordered phase is cubic and magnetically soft. We have exploited this feature and have shown, for the first time, the co-existence of cubic and tetragonal phases, thus giving rise to exchange-coupled spring magnets.

The tensile strength of the alloy specimen is $\sim 50,000$ psi, the highest value among permanent magnets.

- (2) $\text{MnBi}_{1-x}\text{R}_x$ ($\text{R} = \text{Nd}, \text{Dy}$) specimens were prepared to examine the influence of R on the magnetic properties of MnBi. Nearly 30% R could be substituted for Bi. Samples prepared under similar conditions showed that the coercivity of the specimens at room temperature increases from 0.6 kOe for MnBi to ~ 6.4 kOe and ~ 7.8 kOe for Nd and Dy, respectively. Further, the coercivity of the low temperature phase of MnBi increases to a peak value of 25.8 kOe at 280 C.
- (3) Alloys with the composition $\text{RCo}_{7-x}\text{Zr}_x$ were investigated with $\text{R} = \text{Y}, \text{Gd}, \text{Nd}$ or Ho and $x = 0$ to 0.8 . Nearly single-phase materials were obtained with $x = 0.1$ and 0.2 . They stabilize in the TbCu_7 -type structure. Nd and Ho additions significantly modify the magnetocrystalline anisotropy behavior in these systems.
- (4) Band structure calculations on Fe(Co)Pt systems were performed.
- (5) Six publications have resulted from this work.
- (6) Details of the above work are described in this report.

INTRODUCTION

Permanent magnets based on the compositions $\text{Sm}_2\text{Co}_{17}$ and $\text{Nd}_2\text{Fe}_{14}\text{B}$ are employed in the manufacture of a variety of electromechanical devices such as motors, actuators and magnetic bearings. These magnets offer benefits in terms of light-weight and energy efficiency of the finished devices. Further, they provide opportunities to design enabling technologies for military and civilian sectors. Research goals of the program undertaken by Advanced Materials Corporation for the DARPA/ONR initiative are to:

- (a) Develop a deeper understanding of the magnetic properties of materials through a systematic investigation of a few representative alloy systems such as FePt and MnBi.
- (b) Examine the intrinsic properties of rare earth intermetallics such as $\text{RCo}_{7-x}\text{Zr}_x$ and $\text{R}_6\text{Fe}_{11}\text{Ge}_3$, where R is a rare earth metal.
- (c) Examine the prospects of synthesizing bulk Fe_{16}N_2 which has been reported to show a bulk saturation induction of 29 kG – the highest value reported in the literature.

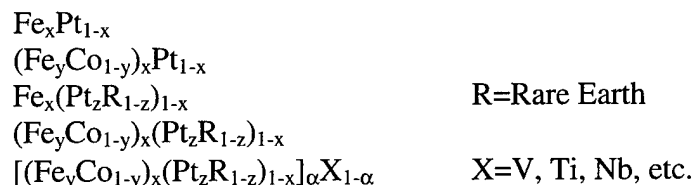
SIGNIFICANT RESULTS

I. Iron-Platinum Alloys

We have employed several processing techniques to produce bulk specimens of Fe-Pt and Fe-Co-Pt. Processing techniques included

- (i) Melt-extracting the bulk specimens in an induction furnace⁽¹⁾,
- (ii) Preparing nanocrystalline powder employing mechanical milling technique at ~ 77 K,
- (iii) Cold rolling as well as hot rolling and
- (iv) Swaging.

We have investigated the following compositions:



Results obtained so far indicate that Fe-Pt magnets obtained through mechanical milling technique provide the highest coercivity (~ 3.5 kOe at room temperature). Cold rolling and swaging techniques also appear to provide bulk magnets with a reasonable coercivity (~ 1.5 kOe). Cold and hot work appears to provide a reasonably fine microstructure.

A representative set of fabrication processes is given in Table I.

Table I. In experiments #6, #7 and #8, the melt is contained in a cylindrical mold and cooled according to the schedule of (a) slow cooled: melt to $\sim 500^\circ\text{C}$ in ~ 8 hours, (b) quenched: melt to solid in ~ 1 minute.

Experiment	Composition	Initial Form	Fabrication process
#1	$\text{Fe}_{60}\text{Pt}_{40}$	powder	Freezer milling of Fe and Pt powders
#2	$\text{Fe}_{60}\text{Pt}_{40}$	ingot	Rf induction melting of Fe and Pt metals
#3	$\text{Fe}_{60.5}\text{Pt}_{39.5}$	ingot	Rf induction melting of Fe and Pt metals
#4	$\text{Fe}_{30.25}\text{Co}_{30.25}\text{Pt}_{39.5}$	ingot	Rf induction melting of Fe, Co and Pt metals
#5	$\text{Fe}_{60.5}\text{Pt}_{35.5}\text{Pr}_4$	ingot	Rf induction melting of Fe, Pr and Pt metals
#6	$\text{Fe}_{60.5}\text{Pt}_{39.5}$	ingot	rf induction melting of Fe metal, Pt metal and powder; slow cooled
#7	$\text{Fe}_{60.5}\text{Pt}_{39.5}$	ingot	rf induction remelting of ingot fabricated in Experiment #3; quenched
#8	$\text{Fe}_{60.5}\text{Pt}_{39.5}$	ingot	rf induction melting of ingot fabricated in Experiment #3; slow cooled

These samples (in both as-fabricated and after heat treatment conditions) have been characterized using X-ray diffraction, TMA, VSM, SQUID and hysteresisgraph. Some of the as-cast alloy samples were then machined and the chips subsequently pulverized to powder form in a mechanical alloying mill at cryogenic temperatures. The resulting fine powders were characterized. Typical results are summarized in tables II and III. X-ray diffraction, TMA, VSM, SQUID and hysteresis loop plots for representative samples are shown in Figs. 1-6.

Table II. Lattice parameters of fct (AuCu) phase of the Fe-Pt systems deduced from x-ray diffraction pattern. For comparison, for FePt, $a = 3.852 \text{ \AA}$ and $c = 3.728 \text{ \AA}$.

Composition	$a (\text{\AA})$	$c (\text{\AA})$
$\text{Fe}_{60}\text{Pt}_{40}$	3.816	3.699
$\text{Fe}_{60.5}\text{Pt}_{39.5}$	3.816	3.677
$\text{Fe}_{30.25}\text{Co}_{30.25}\text{Pt}_{39.5}$	3.791	3.662
$\text{Fe}_{60.5}\text{Pt}_{35.5}\text{Pr}_4$	3.795	3.674

Table III. Magnetic properties of the Fe-Pt based materials obtained by SQUID and hysteresis loop measurements.

Sample	$4\pi M_s$ (kG)	B_r (kG)	H_c (Oe)
Fe ₆₀ Pt ₄₀ Powder > 300 μ m Annealed	13.8 12.8		262 2030
Fe _{60.5} Pt _{39.5} Powder < 38 μ m Annealed	13.3		3600
Fe _{30.25} Co _{30.25} Pt _{39.5} Powder Annealed	12.8		2200
Fe _{60.5} Pt _{35.5} Pr ₄ Powder Annealed	13.6		1700
Fe _{60.5} Pt _{39.5} As Cast	7.5 @ 10 kOe	3.6	888

Measurements of the mechanical properties of FePt magnets indicate that the mechanical strength of these magnets is reasonably high. For example, their tensile strength is superior to the existing (SmCo₅ or Nd₂Fe₁₄B) magnets. Thus, FePt magnets offer a potential for applications in rotating machinery that rotates at very high speed and at high operating temperatures. For example, Fe(Co)Pt possess very high tensile strength as well as reasonably high Curie temperature (See Table IV). SmCo and NdFeB magnets possess relatively low tensile strength due to their lack of ductility.

Table IV. Properties of the Fe-Pt systems. Each sample labeled as 'annealed' has been heated in a sealed tube with partial argon pressure at 600 °C for ~10 hours.

Sample	Phase Present	T_c (°C)	Mechanical Strength	
			BHN (1/16 Ball)	Tensile Strength (psi)
Fe ₆₀ Pt ₄₀ As Cast Annealed	γ fcc γ_1 fct	400 400	97	47900
Fe _{60.5} Pt _{39.5} As Cast	γ fcc		108	53300
Fe _{60.5} Pt _{39.5} Powder < 38 μ m Annealed	γ fcc γ_1 fct	360 450		
Fe _{30.25} Co _{30.25} Pt _{39.5} As Cast Annealed	γ fcc γ_1 fct	615	86	42600
Fe _{60.5} Pt _{35.5} Pr ₄ As Cast Annealed	γ fcc γ fcc + γ_1 fct	300	94	46700
Fe _{60.5} Pt _{35.5} Pr ₄ Powder Annealed		360		

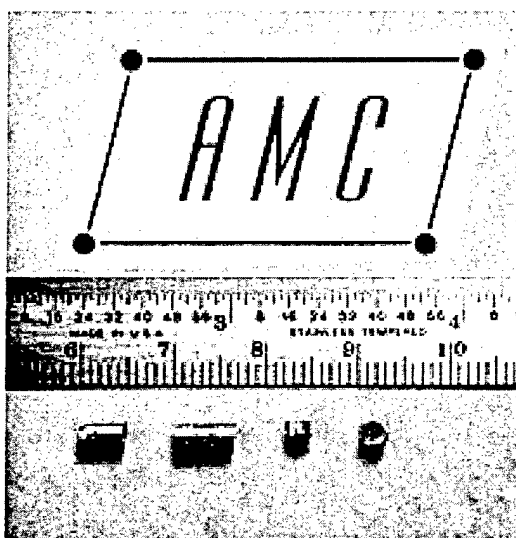


Fig.1: Fe-Pt magnets made by melt extraction

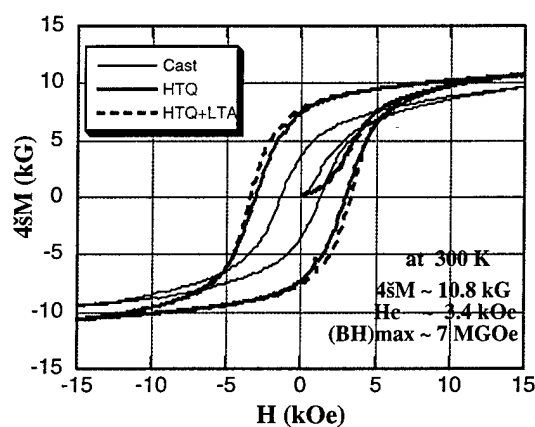
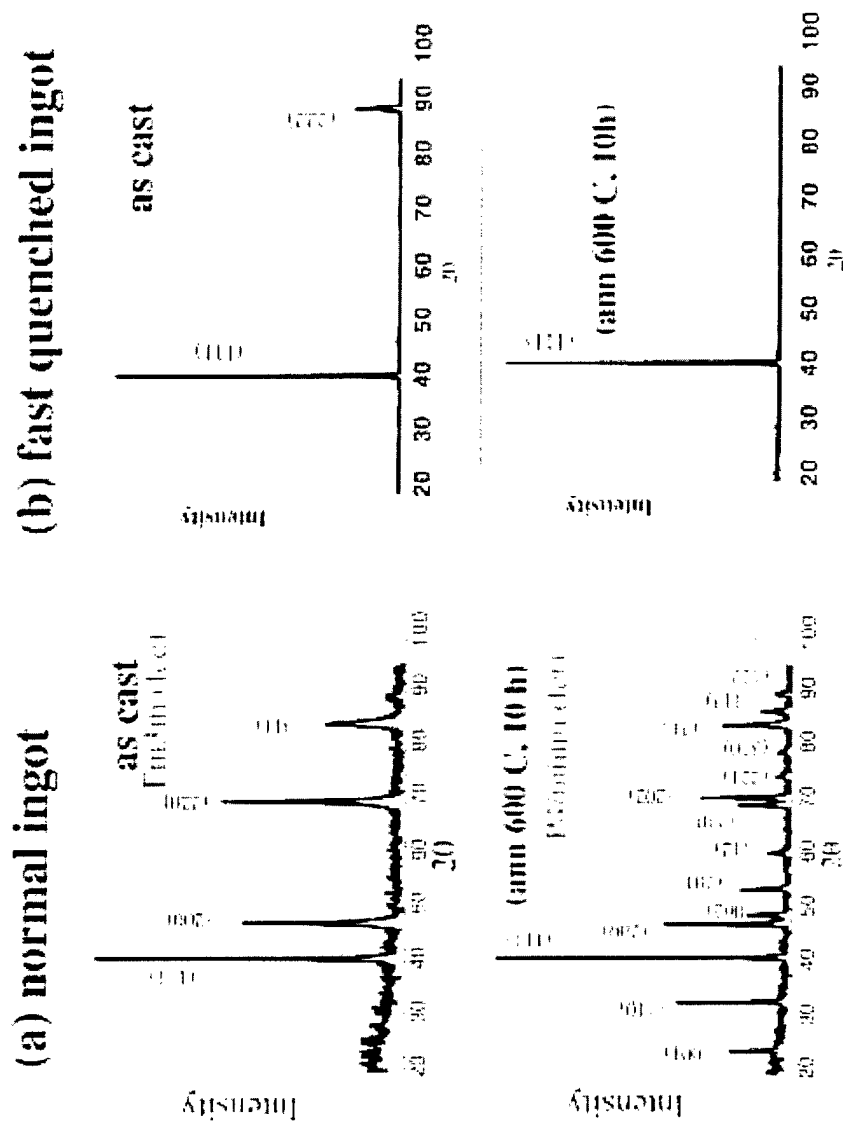


Fig.2. $4\pi M$ -H at RT of Fe-39.5%Pt magnet, (as cast, HTQ and LTA)

Fig. 3. XRD of $\text{Fe}_{0.60}\text{Pt}_{0.40}$ as-cast and heat treated ingot



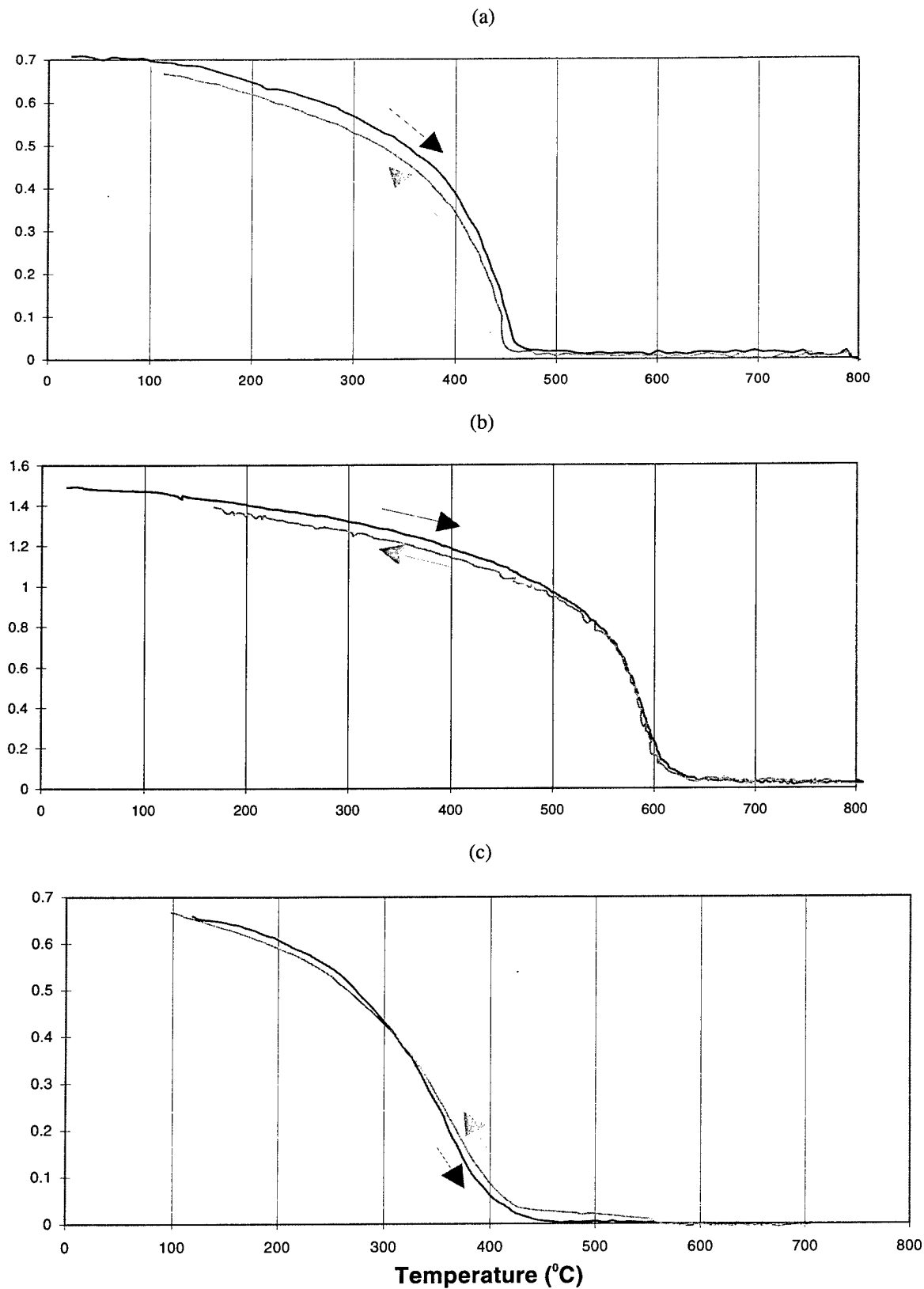
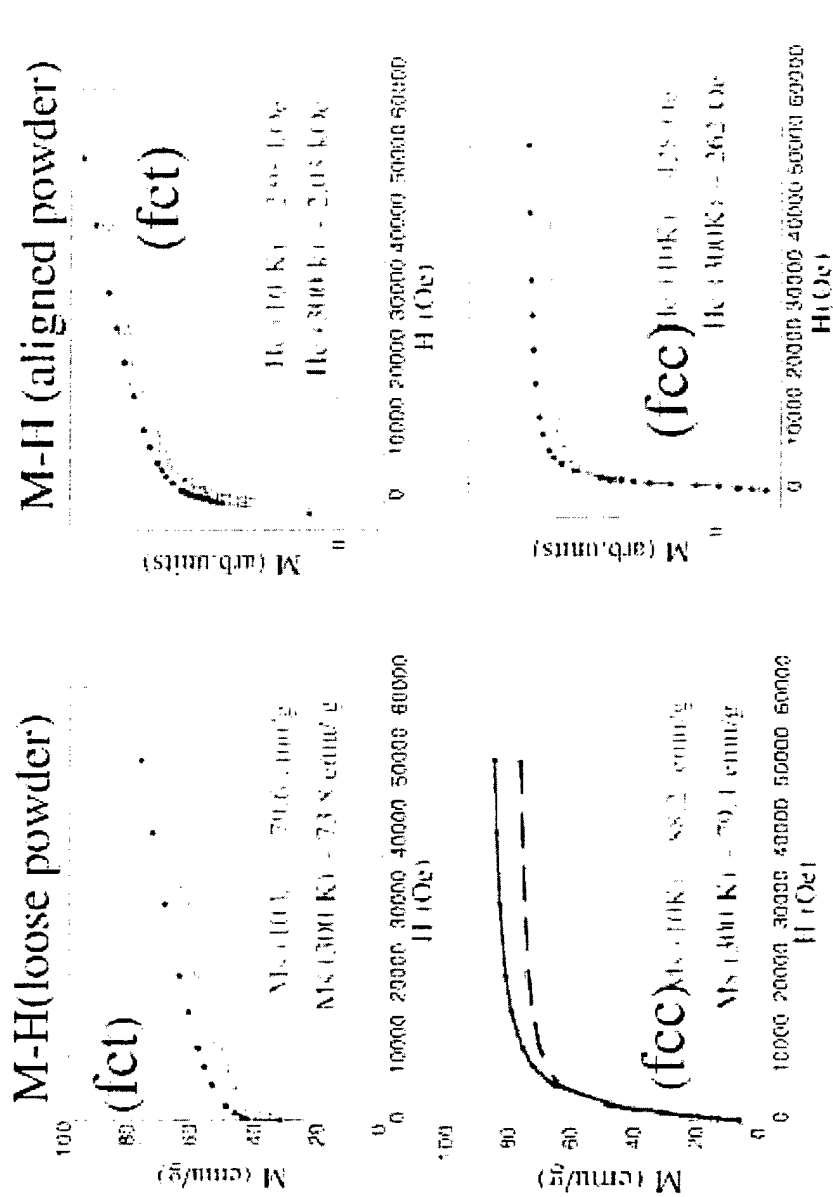


Fig. 4. TMA of (a) $\text{Fe}_{60.5}\text{Pt}_{39.5}$ (b) $\text{Fe}_{30.25}\text{Co}_{30.25}\text{Pt}_{39.5}$ and (c) $\text{Fe}_{60.5}\text{Pt}_{35.5}\text{Pr}_4$ powder samples which have been annealed.

**Fig. 5. M-H of $\text{Fe}_{0.60}\text{Pt}_{0.40}$ as-cast and heat treated powder
(by SQUID)**



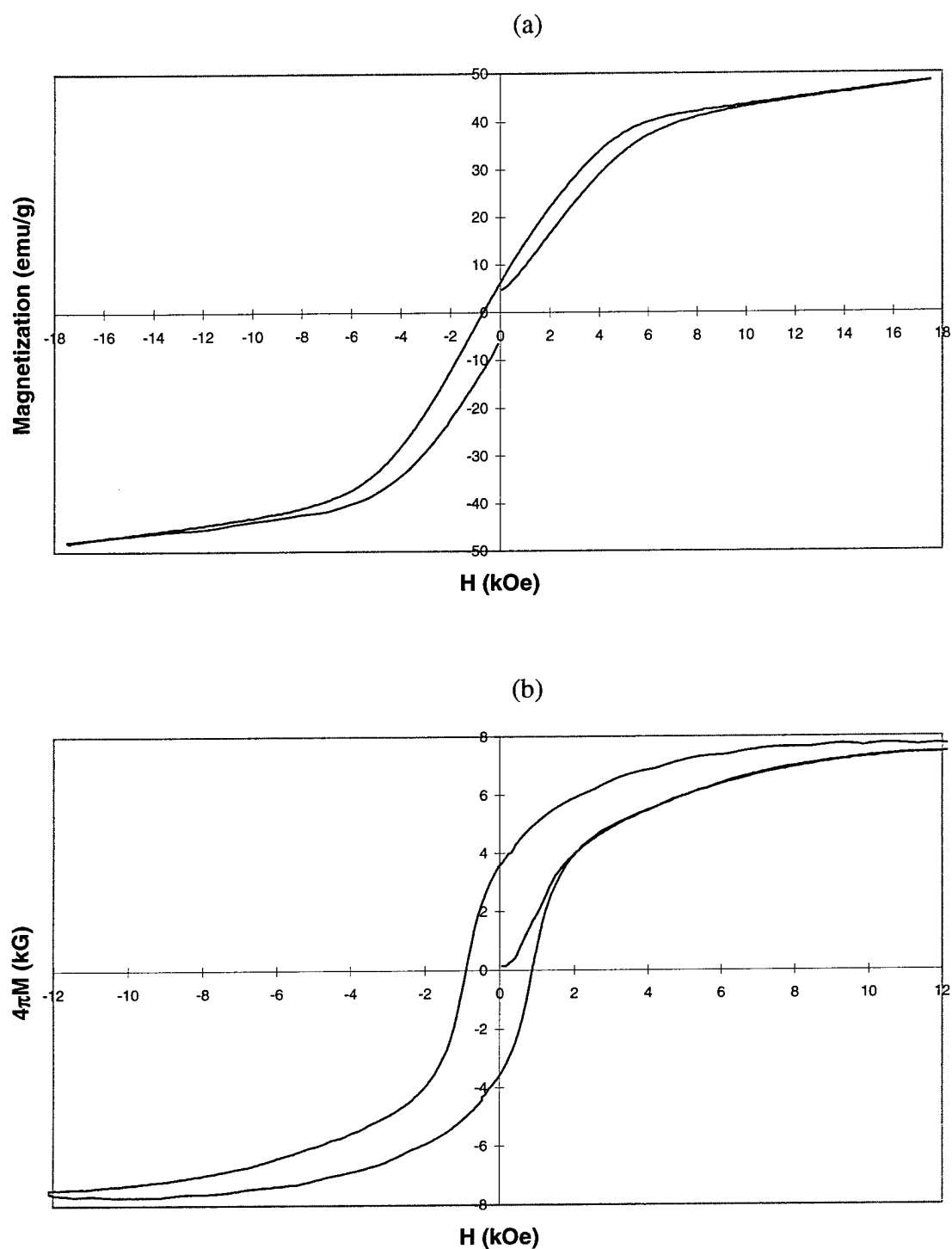


Fig 6. (a) VSM plot of a fast quenched Fe_{60.5}Pt_{39.5} sample and (b) virgin hysteresis loop of a slow cooled as cast Fe_{60.5}Pt_{39.5} ingot magnet.

Spring Magnet

FePt (for 40 ~ 60 at. % Fe) exhibits an order-disorder transformation. The disordered phase crystallizes in a face centered cubic structure and is magnetically soft while the ordered phase is tetragonal and shows high magnetic anisotropy. Since the two structures are coherent, we have an ideal system to investigate the basic features of exchange coupled magnets⁽²⁾. Bulk $\text{Fe}_{0.6}\text{Pt}_{0.4}$ exhibits reasonably large permanent magnetic properties with a maximum energy product of ~15 MG Oe (120 kJ/m^3) without special processes to promote grain alignment. The high energy product is partially a result of the high ratio of remanence to the saturation induction which amounts to 0.68 as opposed to the ratio of 0.5 for an assembly of randomly oriented uniaxial magnets (See Table V and Figure 7). This enhanced remanence is predicted by the exchange-coupled (spring) magnet model for a mixture of cubic and uniaxial phases. In order to verify that the high remanence of the FePt magnets is indeed caused by this exchange mechanism and not by fortuitous formation of magnetic texture during sample preparation, we have prepared cubic samples of $\text{Fe}_{0.6}\text{Pt}_{0.4}$ and measured the B-H loops along the three principal directions of the cube using a VSM (See Figures 8 and 9). The hysteresis loops are identical in all three directions, indicating the absence of strong texture in this material. After correction of the demagnetizing factor, the ratio of remanence to saturation induction is 0.66 ~ 0.68. This is consistent with the exchange coupling model. The highest energy product in our study was found for the as-quenched samples. Further annealing, with the intention to promote formation of the hard magnetic phases, reduced the coercivity and remanence. This suggests that improved results may be achieved by initial suppression of the formation of the hard phases by modification of the quenching process and alloying. The ideal exchange coupled system may be designed based on such a starting material.

Table V. Energy product, remanence, saturation, remanence to saturation ratio and coercivity of as-cast and heat treated samples

$\text{Fe}_{0.6}\text{Pt}_{0.4}$	As Cast			16hrs/600 °C	16hrs/650 °C
	X	Y	Z	Z	Z
BH_{max} (MGOe)	4.87	5.33	5.94	5.36	4.15
B_r (kG)	6.86	7.34	7.63	7.13	6.49
B_s (kG)	10.37	10.92	11.20	10.60	10.36
B_r/B_s	0.66	0.67	0.68	0.67	0.63
H_c (kOe)	2.37	2.34	2.36	2.40	2.11

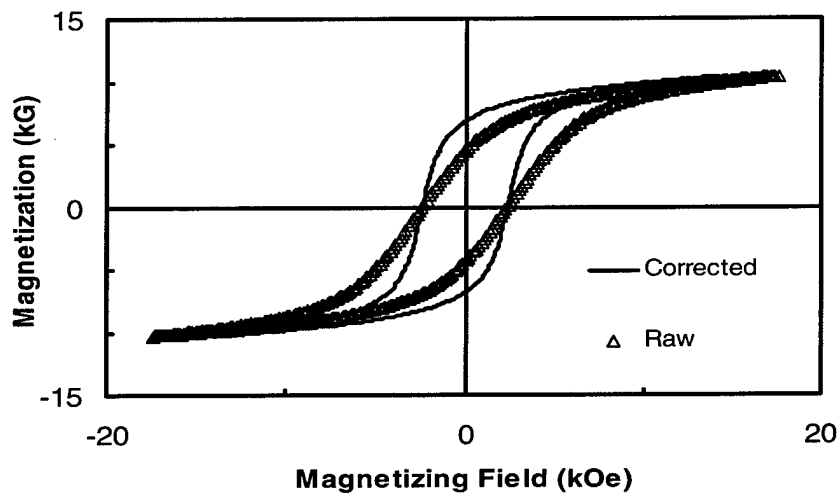


Fig. 7. Raw and corrected z-axis magnetization versus magnetizing field for an as cast sample of Fe-Pt.

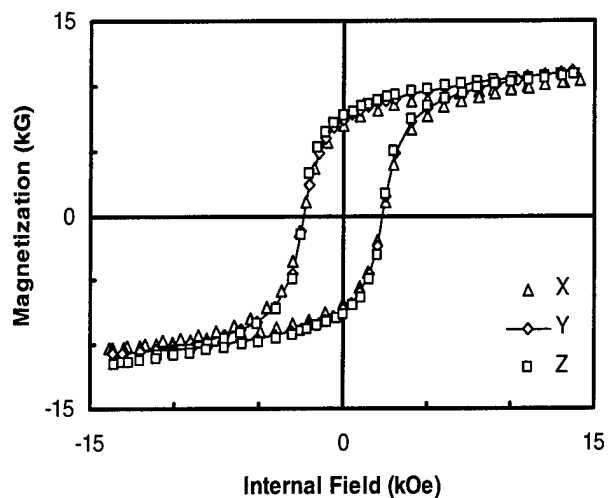


Fig. 8. Magnetization versus internal field for as cast and heat treated FePt for 16 hrs at 600 °C and at 650 °C.

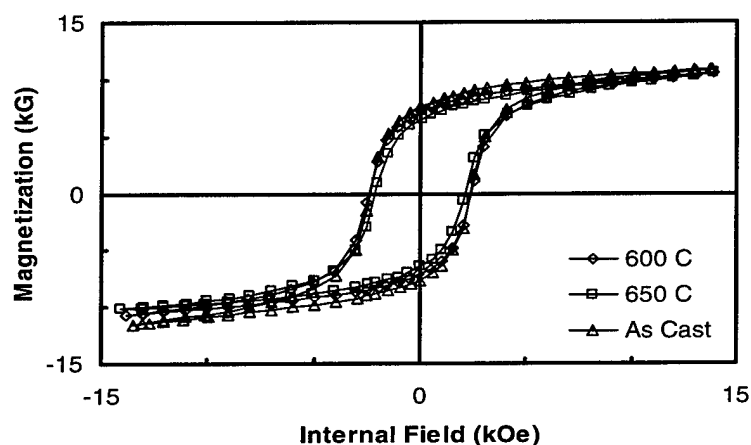


Fig. 9. Magnetization versus internal field along the x, y and z axis for the as cast sample of FePt and along the z axis for the 600 °C heat treatment sample.

Band Structure Calculations

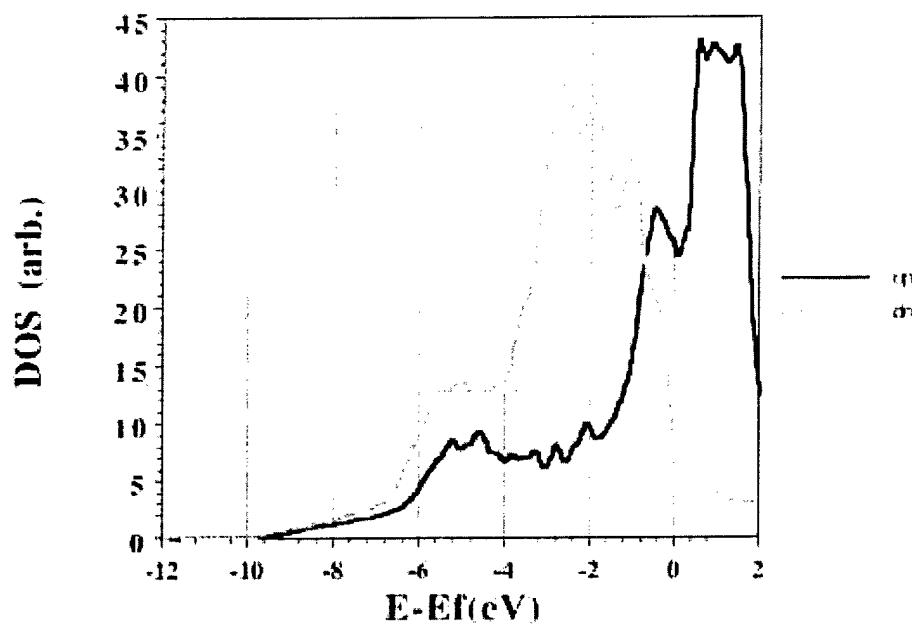
We have undertaken band structure calculations of FePt and MnBi phases using the Layer Korringa Kohn Rostoker (LKRR) band structure technique in the spin-polarized and relativistic modes⁽³⁾. Professor Mike McHenry performed this as a subcontract under this program. The atomic spheres and local spin-density functional (LSDA) approximations were employed. The Von Barth Hedin (VBH) LSDA was employed with a spherical harmonic basis up to $l=3$, and 36 k-points. Densities of states were generated using a 0.005 Ha imaginary (broadening) component of the energy. Magnetic moments and densities of states agree with the literature value of the room temperature FePt and CoPt lattices (See Table VI). The magnetocrystalline anisotropy constants K_1 calculated for FePt and CoPt are in reasonable agreement with published experimental values. Further, these calculations show that the anisotropy constant is quite sensitive to the 'a' lattice parameter. Majority and minority spin densities of states for Fe, Co and Pt in FePt and CoPt are shown in Figures 10 and 11.

Table VI Summary of Magnetic Moments in FePt and CoPt

	Fe(Co) moment μ_B	Pt moment μ_B
FePt	2.917	0.343
CoPt	1.933	0.388

Calculated for $L1_0$ crystal structure $a = 3.852 \text{ \AA}$, $c = 3.723 \text{ \AA}$, $c/a = 0.966$

Fe DOS in L10 FePt



Pt DOS in L10 FePt

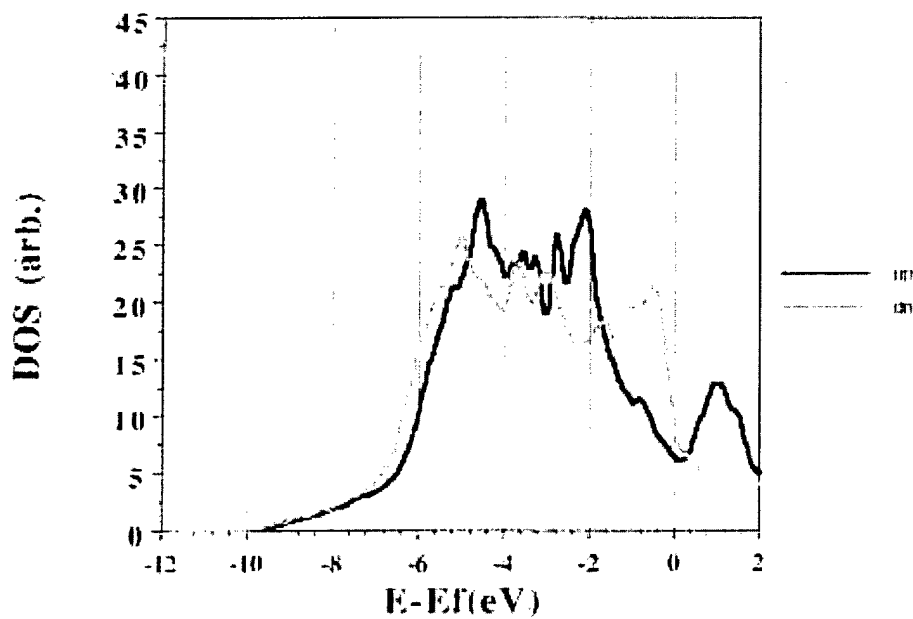


Fig. 10. Density of States for Fe and Pt in FePt (L_{10} crystal structure with $a=3.852 \text{ \AA}$ and $c=3.723 \text{ \AA}$)

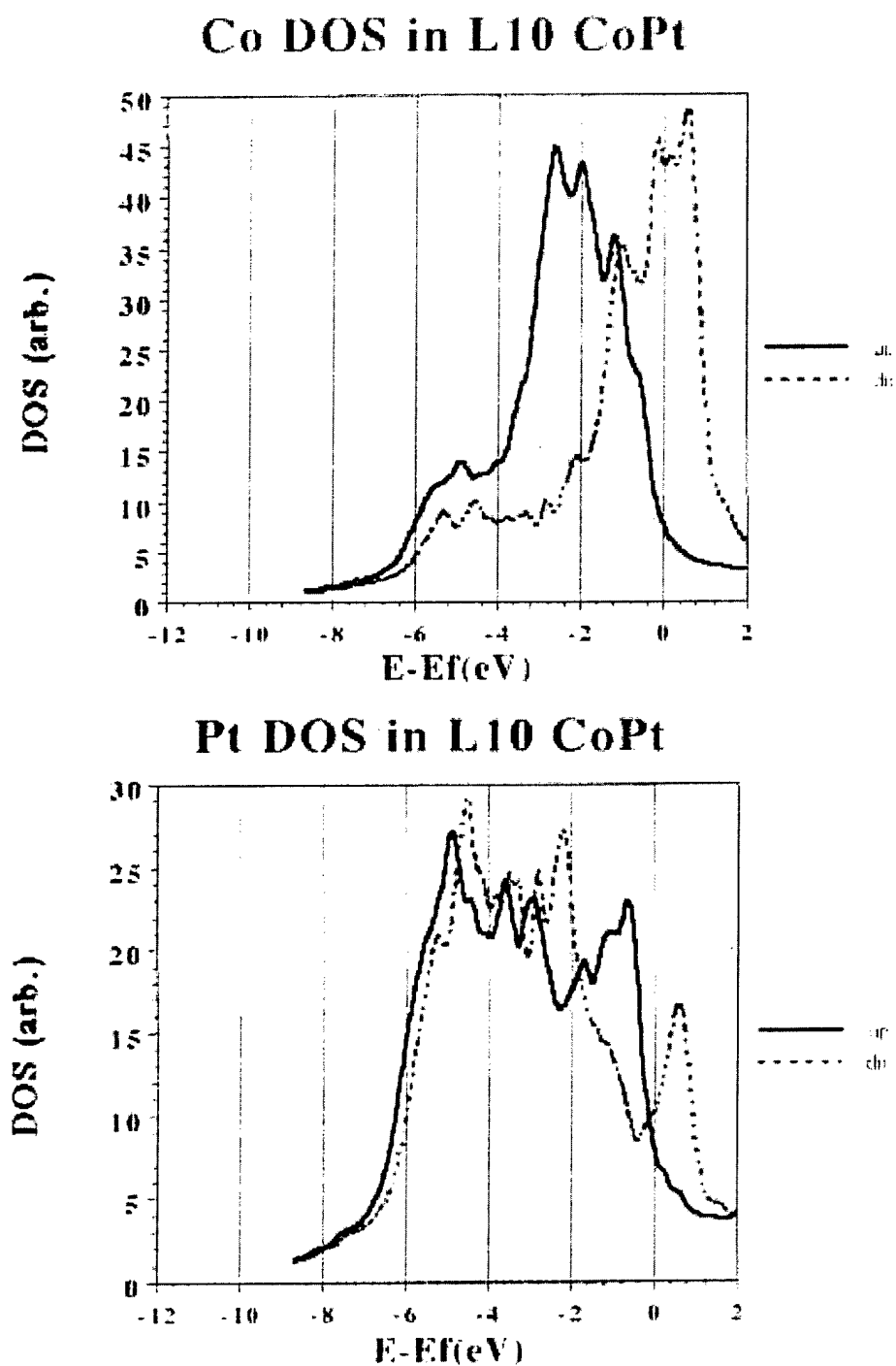


Fig. 11. Density of States for Co and Pt in CoPt (L_{10} crystal structure with $a=3.852 \text{ \AA}$ and $c=3.723 \text{ \AA}$)

II. MnBi Alloys

MnBi crystallizes in a hexagonal NiAs-type crystal structure with a saturation induction B_s of ~ 8.5 kG at room temperature and exhibits a Curie temperature of $\sim 360^\circ\text{C}$ ⁽⁴⁾. MnBi exhibits an unusually large magnetocrystalline anisotropy. The anisotropy field increases with increasing temperature, while in ferromagnetic materials this property usually decreases with temperature. Two forms of MnBi – a low temperature phase (LTP) and a high temperature phase (HTP) – exist. Guo et al.⁽⁵⁾ reported that the LTP phase of MnBi exhibits an increase in the coercivity from 200 Oe at 77K to about 18,000 Oe at 500K.

We have undertaken a systematic examination of the synthesis, structural and magnetic characteristics of MnBi and other modifications with partial incorporation of rare earth ions such as praseodymium, neodymium and dysprosium. We have employed two novel approaches in this research: (1) Obtain nanocrystalline material employing mechanical alloying techniques and compare the results with those obtained through conventional means and (2) perform mechanical alloying at nearly 78K; at such a low temperature, most metals are brittle and are expected to form fine powder.

We have examined the resultant materials using powder x-ray diffraction (under sub-contract with Carnegie Mellon University), DSC and magnetometry. The most striking results are that (1) MnBi in bulk form exhibits an increase in coercivity from 500 Oe at room temperature to 2000 Oe at 573K. This is in accord with the variation of anisotropy field; (2) a large fraction ($>60\%$) of the low temperature phase of MnBi can be easily formed through the use of mechanical alloying (of Mn and Bi) at 78K.

A number of binary and ternary specimens of the composition MnBi, $\text{Mn}_{1-x}\text{Co}_x\text{Bi}$ and $\text{MnBi}_{1-x}\text{R}_x$ (where R is a rare earth element such as Nd and Dy) were prepared. Preparative techniques included melting the constituent elements in an induction furnace as well as mechanical milling. Results obtained in this program may be summarized as follows:

- (i) The coercivity of MnBi increases substantially from ~ 0.1 kOe at 10 K to ~ 16 kOe at room temperature. This trend follows with the enhancement of magnetocrystalline anisotropy field as the temperature of the specimen is increased from 4.2K to room temperature.
- (ii) Due to the high magnetocrystalline anisotropy of rare earth elements, we expected that the partial substitution of Bi by Nd or Dy should increase the anisotropy of MnBi. Thus, we have studied $\text{MnBi}_{1-x}\text{Nd}_x$ and $\text{MnBi}_{1-x}\text{Dy}_x$ for $x = 0.0$ to 0.3. Results of the M vs H measurements on these two systems are shown in Fig. 12 and Fig. 13 respectively. We observe that in $\text{MnBi}_{1-x}\text{Nd}_x$, the coercivity increases from 0.63 kOe to 6.44 kOe for $x = 0.0$ to 0.3 respectively. In $\text{MnBi}_{1-x}\text{Dy}_x$, the coercivity increases from 0.63 kOe to 7.77 kOe for $x = 0.0$ to 0.3.
- (iii) The temperature dependent magnetization on $\text{MnBi}_{1-x}\text{Nd}_x$ and on $\text{MnBi}_{1-x}\text{Dy}_x$ are shown in Fig. 14 and Fig. 15 respectively. In both cases, the increase in the rare earth substitution reduces the sharpness of the transition from Low Temperature Phase (LTP) to High Temperature Phase (HTP). However, the T_c does not change appreciably. On the other hand, on cooling, the HTP-LTP transition

- remains sharp although the transition temperature decreases slowly as rare earth concentration increases.
- (iv) We have made an effort to examine the possibility of raising the Curie temperature of the MnBi system. Fig. 16 shows data for the $\text{Mn}_{0.8}\text{Co}_{0.2}\text{Bi}$ compound. We see that the usual LTP-HTP transition around 360 C for MnBi is not present; instead $\text{Mn}_{0.8}\text{Co}_{0.2}\text{Bi}$ shows a two-step transition at 467 C and at 524 C. However, the HTP-LTP transition occurs at 258 C, which is about 60 C lower than that of MnBi. A subsequent measurement eliminates the two high temperature transitions and gives only one transition. It appears that in $\text{Mn}_{0.8}\text{Co}_{0.2}\text{Bi}$ some metastable states are present which destabilize on repeated heat treatment.
 - (v) MnBi magnets have been prepared. MnBi was prepared by freezer-milling in liquid nitrogen. The collected powder was then isostatically pressed and later heat treated for different time duration from 2 hours to 10 days at different temperatures from 265 C to 440 C. The annealed compound was then ball-milled for 24h and subsequently magnetized and isostatically pressed to make cylindrical shaped magnet. A coercivity of 9.7 kOe was achieved. The maximum saturation induction was 0.23 kG. Fig. 17 shows a typical hysteresis loop for the MnBi magnet.
 - (vi) Addition of cobalt decreases the Curie temperature of MnBi.

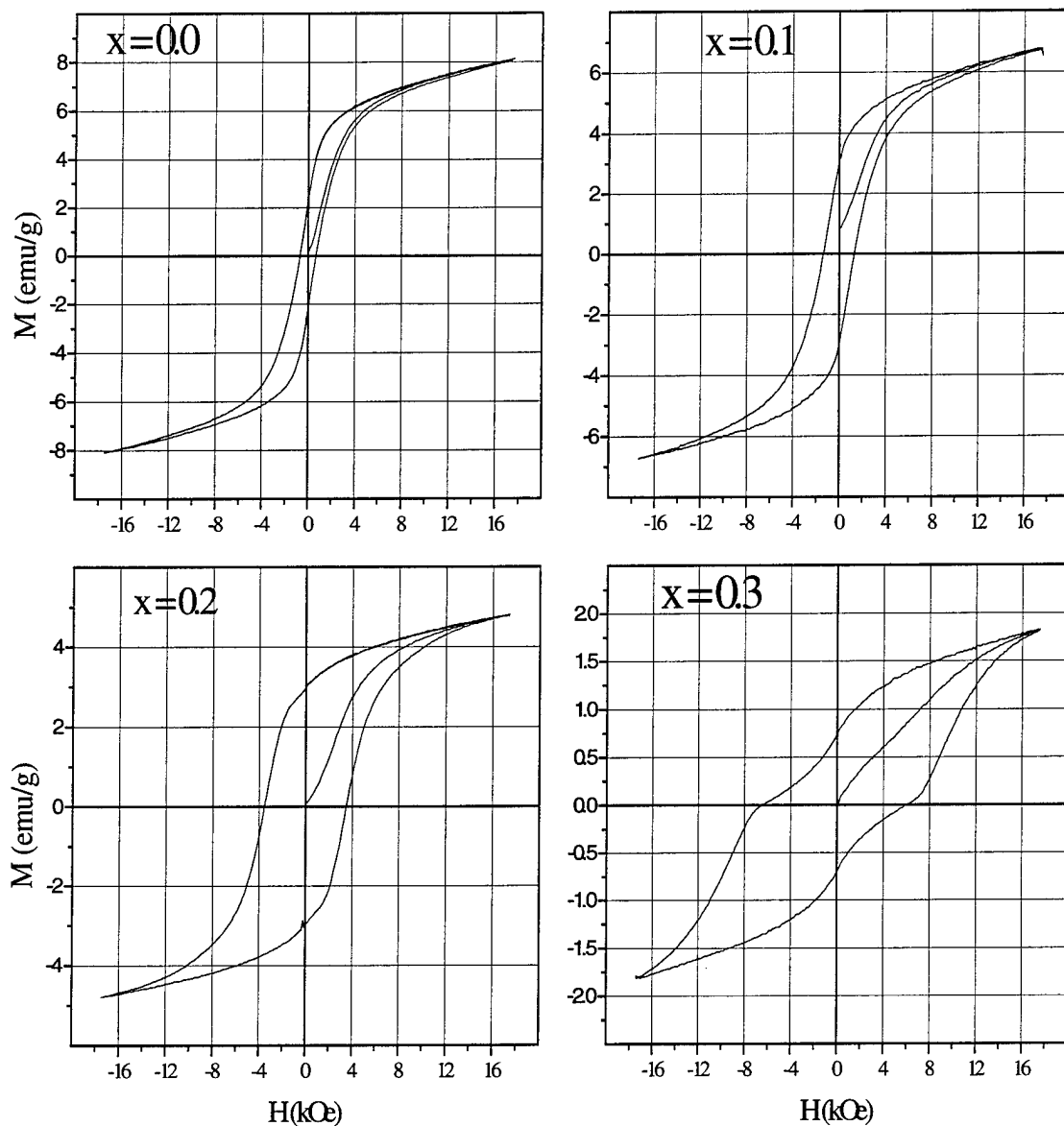


Fig 12. Magnetization vs. External Field for $\text{MnBi}_{1-x}\text{Nd}_x$.

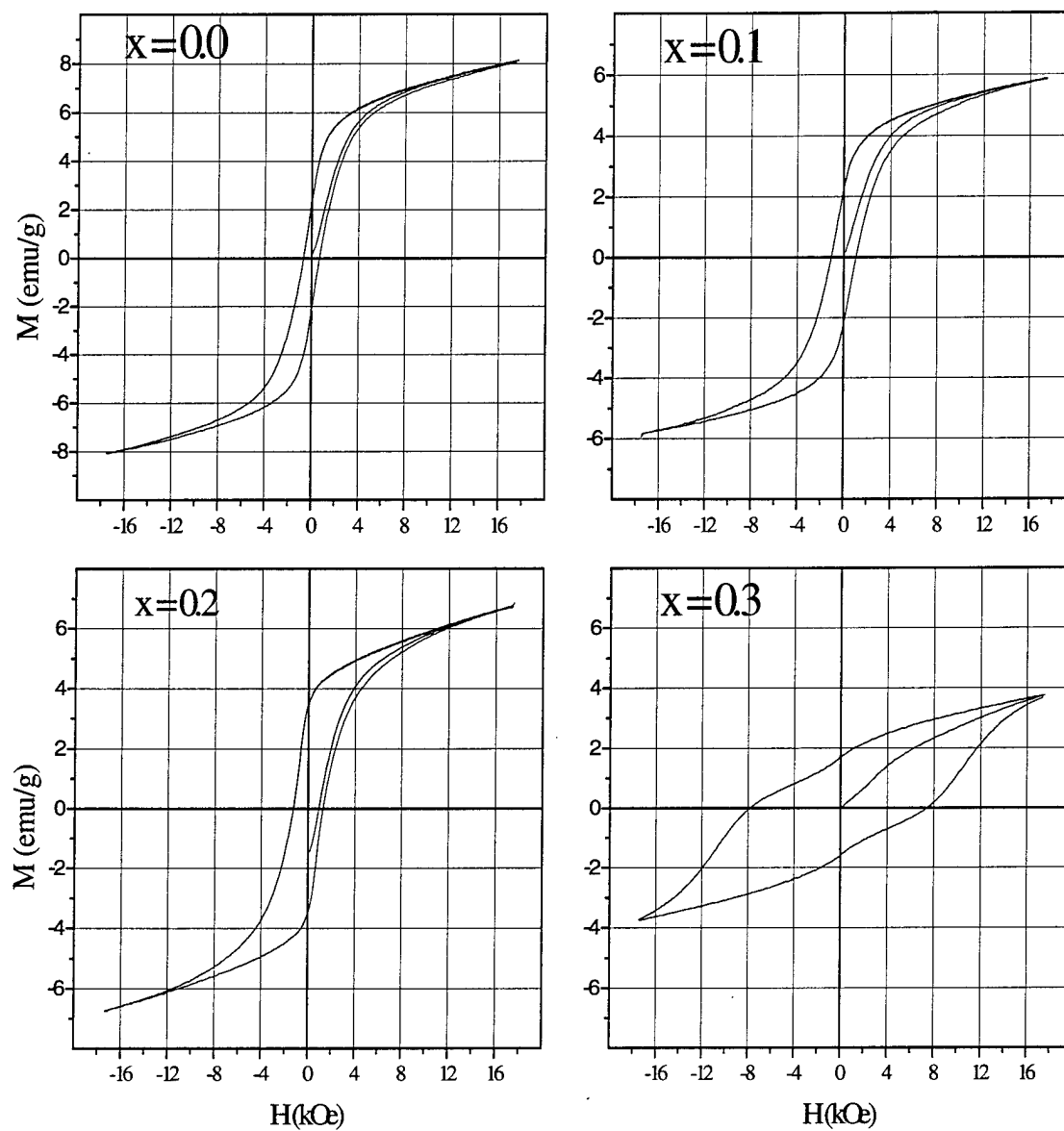
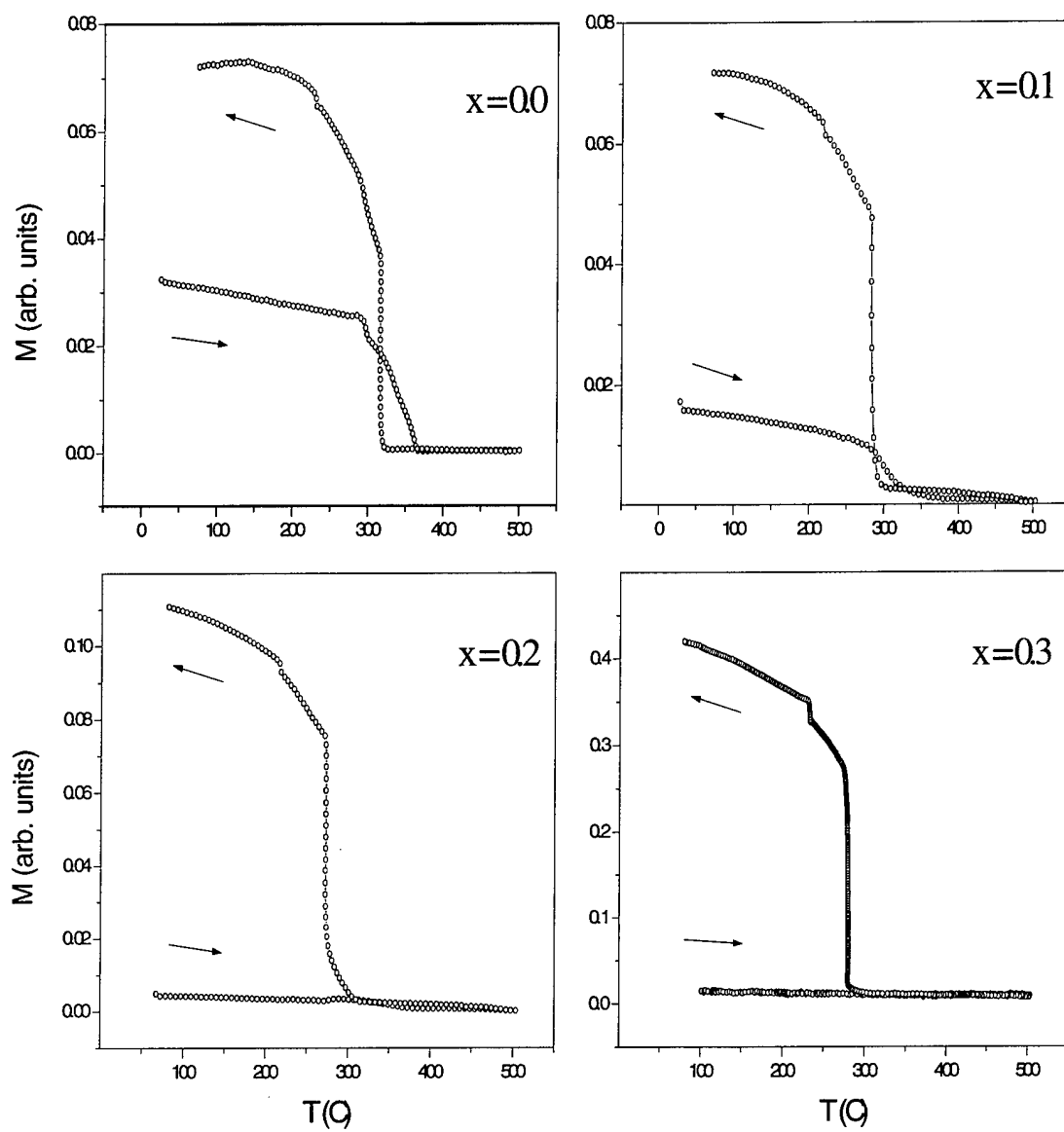


Fig. 13. Magnetization vs. External Field for $\text{MnBi}_{1-x}\text{Dy}_x$

Fig. 14. Magnetization vs. Temperature for $\text{MnBi}_{1-x}\text{Nd}_x$

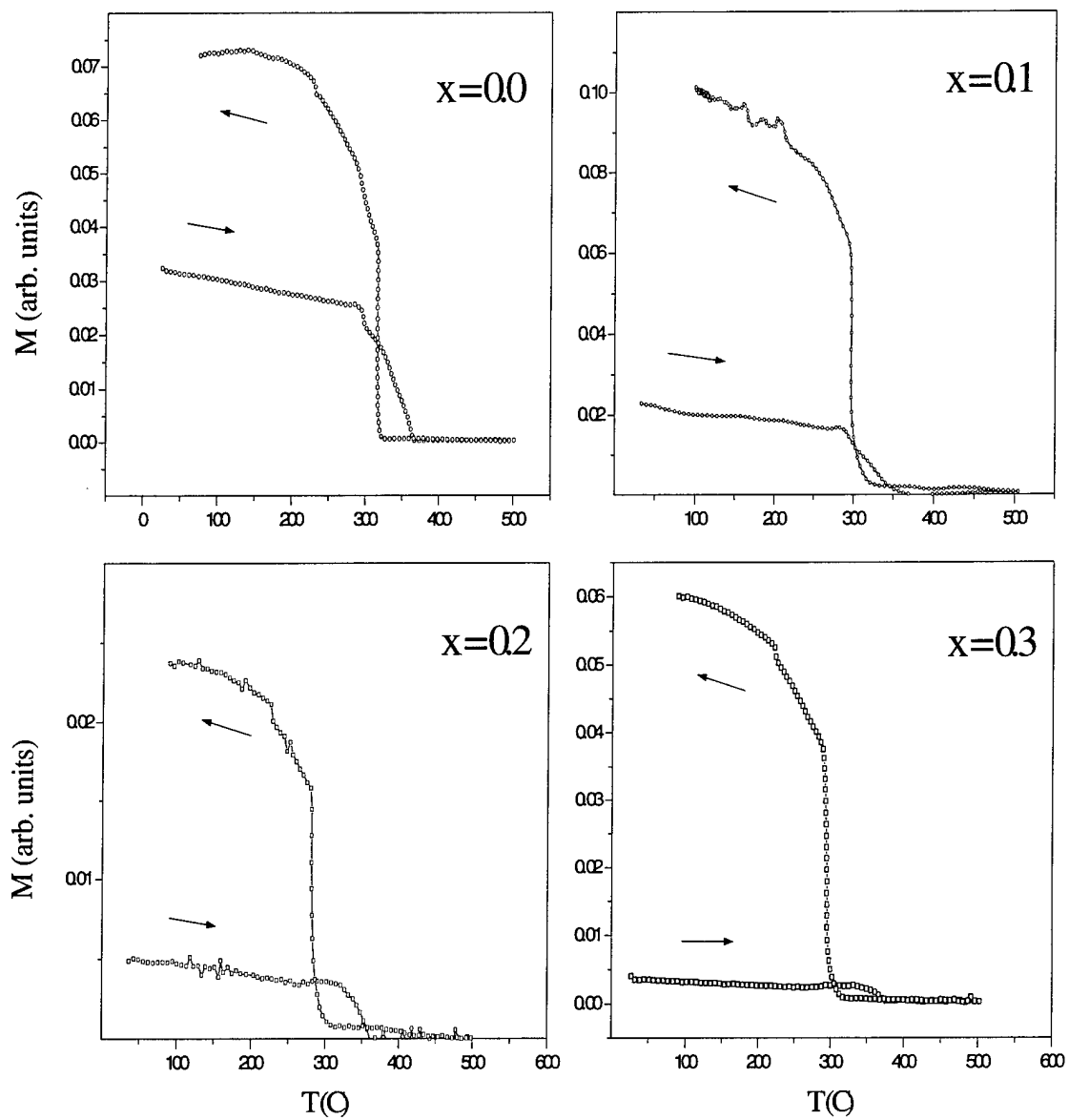


Fig. 15. Magnetization vs. Temperature for $\text{MnBi}_{1-x}\text{Dy}_x$

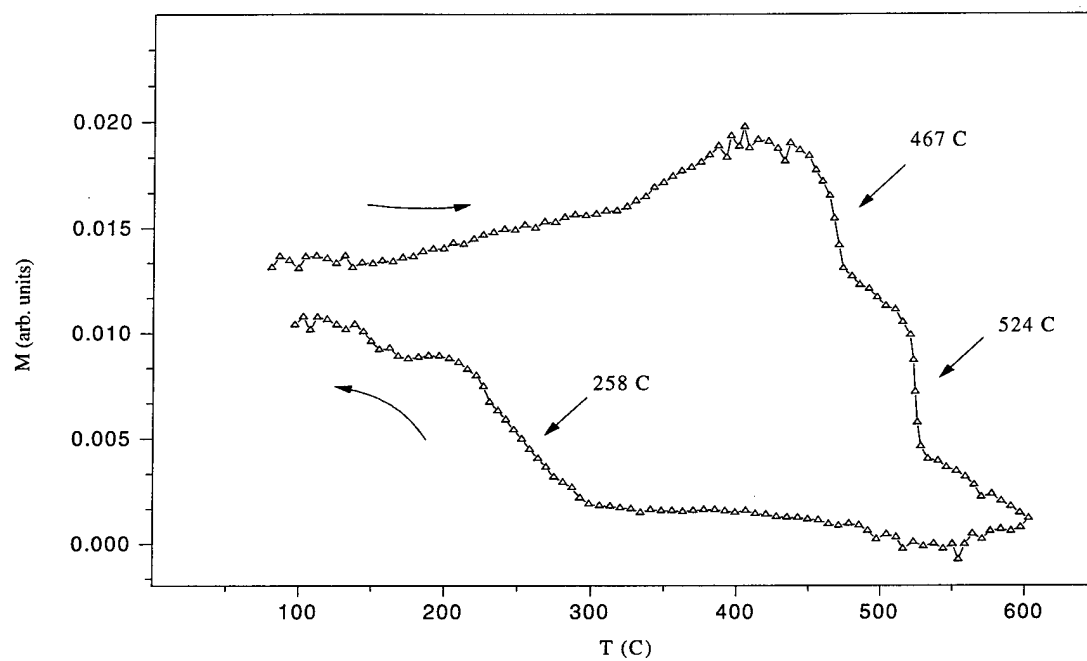
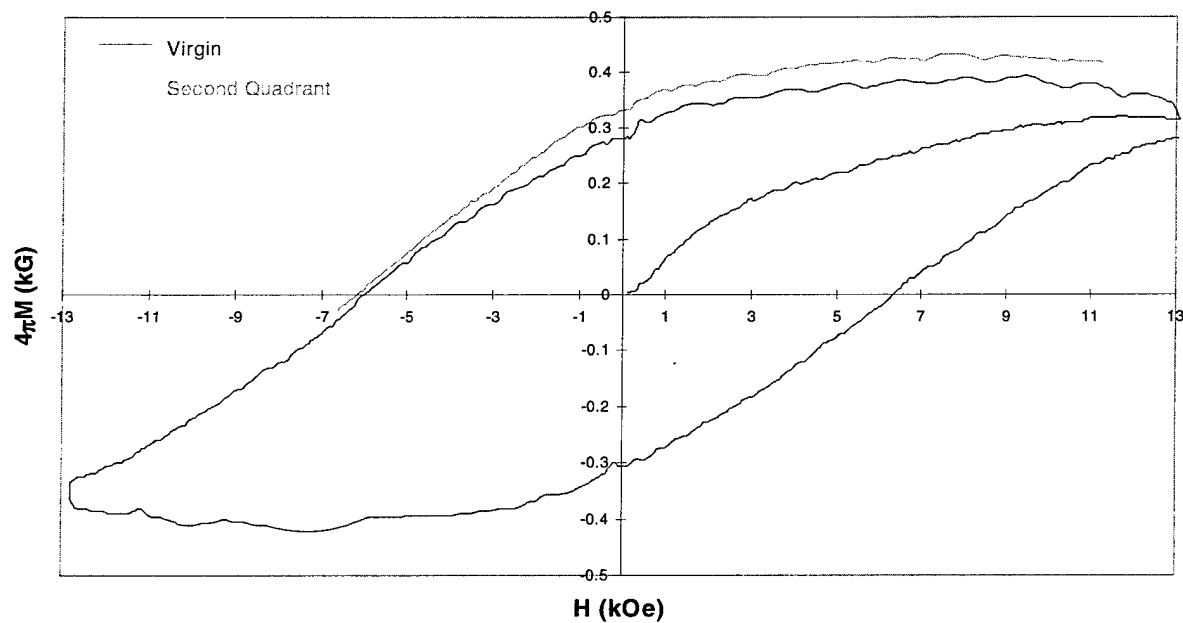
Fig. 16. Magnetization vs. Temperature for $\text{Mn}_{0.8}\text{Co}_{0.2}\text{Bi}$ 

Fig. 17. Hysteresis Loop for a MnBi Magnet

III. $\text{RCo}_{7-x}\text{Zr}_x$ Systems ($\text{R}=\text{Y}, \text{Nd}, \text{Gd}$ or Ho)

In a search for new type of high performance magnetic materials (hard and soft), we have examined a number of compositions such as (i) $\text{R}(\text{Co}, \text{Fe})_{7-x}\text{M}_x$, (ii) $\text{R}_6\text{Co}_{11}\text{M}_3$ and (iii) Fe-N systems.

In this context, alloys of the compositions $\text{RCo}_{7-x}\text{Zr}_x$, with $\text{R} = \text{Y}, \text{Nd}, \text{Gd}$ and Ho , $x=0$ to 0.8 , have been investigated. In these compositions, the magnetic anisotropy arises mostly from the Co sublattice. Nearly single phase disordered TbCu_7 structure forms in the as-cast alloys when $x=0.1$ and 0.2 . In the case of $\text{R}=\text{Y}$ and Gd , a large increase in the anisotropy field was observed with Zr doping. For $\text{R}=\text{Y}$, the anisotropy field increases from 18 kOe for $x=0$ to 74 kOe for $x=0.2$ at room temperature and from 20 kOe at $x=0$ to 82 kOe for $x=0.2$ at 10 K. In the case of $\text{R}=\text{Nd}$ and Ho , the rare earth sublattice prefers a planar anisotropy at room temperature. We have also observed spin reorientation phenomena in some of these materials. These results were published in the Journal of Applied Physics.

Our current understanding of these families of materials may be summarized as follows:

- 1) Zr plays an important role in stabilizing the TbCu_7 structure in $\text{RCo}_{7-x}\text{Zr}_x$ alloys⁽⁶⁾.
- 2) Zr replaces the Co dumbbells and significantly increases anisotropy.
- 3) Experimental anisotropies for the Sm, Pr and Er-based materials are in line with the expectations derived from crystal field interactions and their influence on the magnetocrystalline anisotropy in rare earth intermetallics. For example, the x-ray diffraction patterns of the holmium analog show basal plane anisotropy (See Figure 20).
- 4) $\text{RCo}_{7-x}\text{Zr}_x$ or $\text{R}(\text{Co}, \text{Fe}, \text{Cu}, \text{Zr})_7$ are new candidates for permanent magnetic materials to improve the high temperature magnetic properties of current 2-17 magnets. A large increase of H_c was observed in the $\text{Sm}(\text{Co}, \text{Fe}, \text{Cu}, \text{Zr})_7$ alloys; after heat treatment H_c increases from 1.9 kOe to 15 kOe at RT and from 21 kOe to near ~50 kOe at 10 K. Doping SmCo_7 with a small amount of Cu improves the anisotropy in SmCo_7 . As x increases from 0 to 0.1 in $\text{SmCo}_{7-x}\text{Cu}_x$, the anisotropy field increases from 90 kOe to 130 kOe (at room temperature) and from 140 kOe to 230 kOe at 10 K.

Electron Energy Corporation has, independently, begun manufacturing magnets based on these compositions⁽⁷⁾.

Representative results are given in Table VII.

Table VII. Structure and Magnetic Properties of $\text{RCo}_{7-x}\text{Zr}_x$ (as cast or annealed)
($\text{R}=\text{Y}, \text{Pr}, \text{Nd}, \text{Sm}, \text{Gd}, \text{Tb}, \text{Dy}, \text{Ho}, \text{Er}, \text{La}$)

Composition	Structure	T_c (C)	M (emu/g) at RT	H_a (kOe) at RT
$\text{YCo}_{6.9}\text{Zr}_{0.1}$	1-7(a)	~841	~115	~50
$\text{PrCo}_{6.8}\text{Zr}_{0.2}$	1-7	~690	~112	~95
$\text{NdCo}_{6.8}\text{Zr}_{0.2}$	1-7	~710	~121	~ planar
$\text{SmCo}_{6.8}\text{Zr}_{0.2}$	1-7	~760	~100	~130

GdCo _{6.9} Zr _{0.1}	1-7	~871	~50	~113
TbCo _{6.9} Zr _{0.1}	2-17(c), 1-7	~865	~53	~ planar
DyCo _{6.9} Zr _{0.1}	1-7	~855	~55	~50(planar)
HoCo _{6.9} Zr _{0.1}	1-7	~851	~69	~65
ErCo _{6.9} Zr _{0.1}	1-7	~849	~67	~95
LaCo _{6.7} Zr _{0.3}	1-5(b), 2-17(d)	~ 565, 790	~92	~90
LaCo _{6.7} Ti _{0.3} (ann)	2-17(d)	~610	~92	~25

(a)-TbCu₇, (b)-CaCu₅, (c)-Th₂Ni₁₇, (d)-Th₂Zn₁₇

In LaCo_{7-x}Zr_x systems, we have found that instead of partly replacing dumbbell Co atom pair and stabilizing the TbCu₇ structure, Zr atoms prefer to replace the La atoms and stabilize the CaCu₅ structure. The alloys with $x=0.3\sim 0.8$ exhibit strong uniaxial anisotropies with $H_A=90\sim 100$ kOe at both 300 K and 10 K (Fig18) and $T_c \sim 560$ C.

It is interesting to note that in the LaCo_{7-x}Ti_x system, the alloys with a main phase with the Th₂Zn₁₇ structure were formed when $x=0.3\sim 0.8$ and exhibit a uniaxial anisotropy with $H_a \sim 25$ kOe at both 300K and 10 K. The Curie temperatures are in the range of $625 \sim 710$ C (Fig 19). It can be suggested that in the LaCo_{7-x}Ti_x system, Ti atoms partly replace dumbbell Co atom pair stabilizing the ordered 2-17 structure (Th₂Zn₁₇ structure), but not stabilizing the disordered 2-17 structure (TbCu₇ structure).

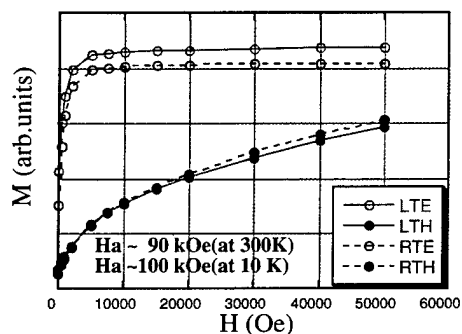


Fig.18. M-H of LaCo_{6.7}Zr_{0.3}-cast

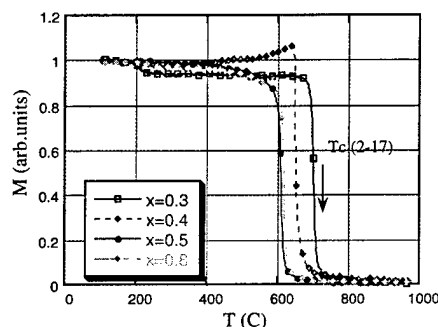


Fig.19. M-T of LaCo_{7-x}Ti_x- ann ($x=0.3-0.8$)

IV. $R_6(Fe, Co)_{11}M_3$ Systems (R =rare earth, M = Ga, or Ge)

$R_6Fe_{11}Ga_3$ compounds crystallize in $La_6Co_{11}Ga_3$ -type structure, which has tetragonal symmetry with space group $I4/mcm$. It was found that $R_6Fe_{11}Ga_3$ alloys with $R=Sm$, Pr or Nd exhibit large anisotropies (~ 7 T) at room temperature. Their Curie temperatures are between 320 and 462 K.

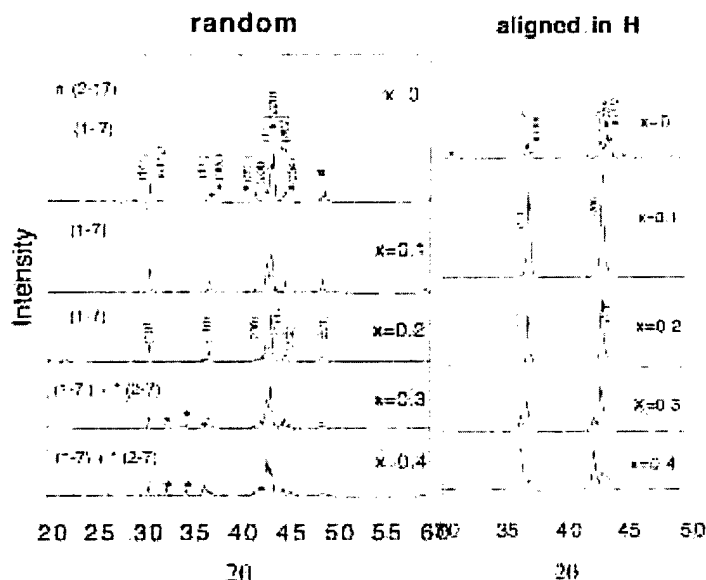


Figure 20 XRD of $HoCo_{7.5}Zr_{1.5}$ as-cast alloys (measured in random and aligned powder)

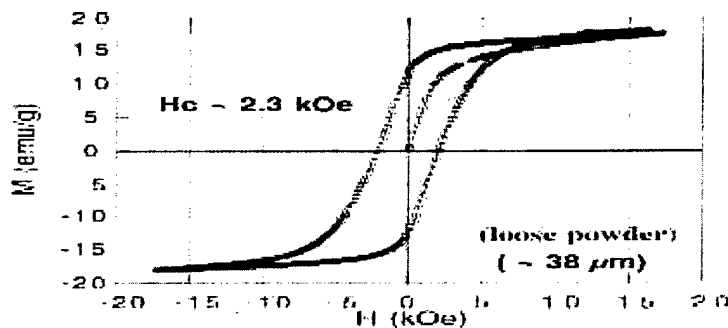


Figure 21 M-H at RT of $La_6Co_{11}Ga_3$ as-cast alloy

Alloys with composition of $R_6Fe_{11}Ga_3$ ($R=Sm$, Pr or Nd) and $R_6Co_{11}Ga_3$ (or Ge) ($R=La$ or Pr) have been examined. For example, $La_6Co_{11}Gd_3$ (as cast) alloy exhibits a $T_c \sim 573$ K and a strong uniaxial anisotropy at room temperature with $H_c \sim 2.3$ kOe for loose powder ($\sim 38 \mu_B$ per formula unit) (See Figure 21).

V. Iron Nitrides

In an effort to synthesize bulk Fe_{16}N_2 , we have examined a number of approaches. One of the precursors needed for this is FeOOH . In the following, we describe the method we used to prepare this material.

(1) Preparation of FeOOH

The starting material used for the nitriding experiments is a finely divided iron oxide hydroxide precipitate. The precipitant solution is prepared by dissolving iron nitrate, $\text{Fe}(\text{NO}_3)_3 \cdot 9\text{H}_2\text{O}$, in distilled water at the ratio of 100g to 1000ml of water. The solution is heated to 80 °C and constantly agitated. Adding ammonia hydroxide solution to the heated iron nitrate solution forms the precipitate. A red-brown precipitate forms instantly. The pH of the solution is monitored and the precipitation reaction is stopped at a pH of 10. The precipitate is recovered by vacuum filtration and dried at 50 °C in a vacuum oven. The dried precipitate is hand ground in a mortar and pestle. Further classification involves sieving the ground precipitate through a 400-mesh sieve.

A second precipitate was prepared similarly but doped with 5w% chromium. Chromium nitrate was added to the precipitant solution along with the iron nitrate. The co-precipitation was carried out as described above.

Both precipitate samples were characterized by x-ray diffractometry. The resulting diffractograms showed broad, low intensity peaks indicating the precipitate consists of very small particle size material. The low intensity peaks are consistent with the structure of FeOOH . There is a likelihood of some Fe_2O_3 and FeO also being present.

(2) Nitrogenation of FeOOH

All of the nitriding experiments were conducted using a custom made retort tube furnace. The retort is provided with the necessary tubing and valves for the introduction of gases at known flow rates. The flow meters are calibrated in cc/min using a Buck Scientific calibration meter. The retort tube is also fitted with a line for a mechanical vacuum pump. A pressure/vacuum compound gauge as well as a thermocouple vacuum gauge are connected to the system.

A known amount of the precipitate was introduced into the hot zone of the furnace. The furnace was slowly ramped to 110°C under vacuum for 10-15 hours. The precipitate is known to decompose slightly as the temperature increases. This is why the initial heating is done under vacuum. After dwelling at 110°C for a few minutes, the furnace is ramped up slowly to 450°C. As the temperature approaches 400°C, hydrogen gas is introduced into the retort. The hydrogen serves to reduce the precipitate to iron powder. The reduction is carried out for one half hour at 450°C. The furnace then is ramped up slowly to the target reaction temperature (640°-680°C). At some point during this ramping, the sample is pulled out of the furnace hot zone. The ammonia/hydrogen flow is started and allowed to stabilize as the target temperature is approached. Once the target reaction temperature is stable, the sample is pushed back into the hot zone and the reaction starts. After the allotted reaction time, the sample is quickly pulled

from the furnace hot zone and rapidly quenched using a stream of high flow helium gas. The gas flow quenching is continued for about 15 minutes. Once the helium quench is complete, the sample cools further in the chilled water-jacketed end of the retort tube. After some time, the sample is removed and prepared for characterization by x-ray diffraction and thermo-magnetic analysis.

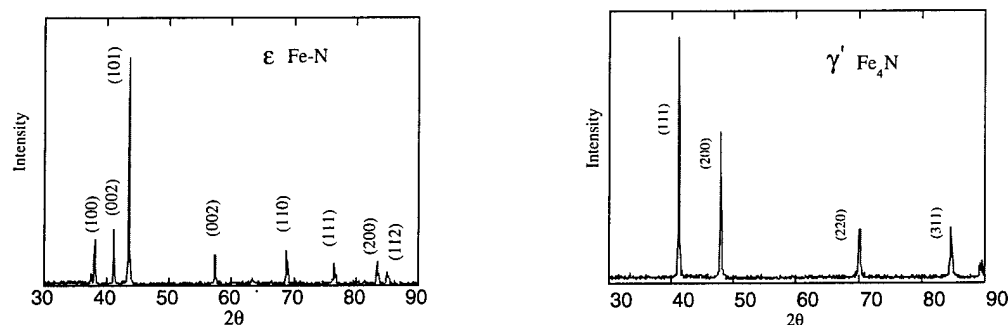
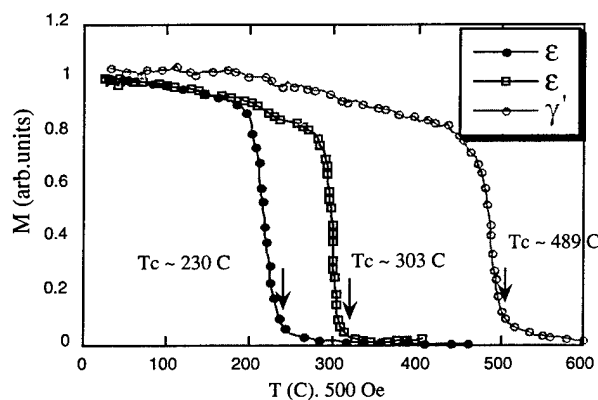
(3) γ -phase as a precursor

We have carried out several studies to synthesize pure α'' -Fe₁₆N₂ using the γ -phase as the precursor. These studies included reaction between iron powder ($\sim 6\mu\text{m}$) and a flowing mixture of NH₃ and H₂ at temperatures between 650~ 670 C. The reaction is followed by tempering at 120 to 130 C to obtain a large fraction of α'' - Fe₁₆N₂. Up to date, the results obtained in our laboratory indicate that we were able to obtain a large fraction (>50%) of α'' - Fe₁₆N₂.

(4) ϵ Fe-N or γ' Fe₄N phase as a precursor.

We have carried out a study on the synthesis of α'' - Fe₁₆ N₂ using the ϵ Fe-N or γ' Fe₄N phase as the precursor. The advantage of this approach is that it enables the incorporation of a larger amount of nitrogen (>10.7 at%) at lower temperatures. On the other hand, γ -Fe phase has a lower solubility of nitrogen and therefore results in the formation of nitrogen-deficient α'' -Fe₁₆N₂. The starting material used for nitrogenation experiments is the FeOOH described earlier. This was first reduced to α -Fe by flowing H₂ at ~ 400 C, followed by a nitrogenation procedure. The nitrogenation was performed by treating the α -Fe fine powder with a mixture of NH₃-H₂ gas at ~ 1 atm. pressure and at temperatures in the range of 640-670 C for 2-3 hours. This material was then quenched to room temperature by helium gas. A single phase material of ϵ Fe-N or γ' Fe₄N was formed. It was confirmed by X-ray diffraction and magnetic measurements (Fig.22 and 23). The nitrogen contents can be varied by changing the ratio of the NH₃ / H₂ and the nitrogenation temperatures. The Curie temperature in the ϵ Fe-N phase varies from 230 C to 300 C as the nitrogen concentration changes about 2~3 at %.

The ϵ Fe-N and γ' Fe₄N fine powder samples subsequently were annealed at 140-170 C for a long time (~ 28 days). We expected that the α'' -Fe₁₆N₂ phase could be precipitated out from ϵ or γ' phase by slow diffusion of nitrogen atoms. However, our results indicate that after annealing the high N content (~ 23 at %) powder at 140 C for 28 days, the α'' - Fe₁₆N₂ phase has

Fig. 22. XRD of ϵ Fe-N and γ' Fe₄NFig. 23. M-T of ϵ Fe-N and γ' Fe₄N

not been detected by x-ray diffraction experiments. It suggests that the high N content ϵ (or γ') phase is still stable at 140 C.

Thus, in spite of several approaches, we were only successful in synthesizing Fe₁₆N₂ in combination with other phases. However, our attempts to prepare this material in pure form proved unsuccessful⁽⁸⁾.

SUMMARY

The objective of this work is to examine the structural and magnetic properties of materials that are of interest in high performance magnets. During the program, a number of alloys have been investigated.

- (1) Fe-Pt based alloys were examined with a view to develop a process to fabricate bulk permanent magnets and to examine the effects of order-disorder phenomena on the permanent magnet properties. Compositions close to $\text{Fe}_x\text{Pt}_{1-x}$ ($x = 0.5$ to 0.615) were prepared by (a) melt-extracting stoichiometric quantities of metals in an induction furnace, (b) mechanically milling the sample at ~ 77 K and (c) by melt spinning technique. Measurements of magnetic properties of these specimens show a typical saturation magnetization of 13.8 kG and 13.3 kG in fcc and fct phases respectively. The corresponding coercivities are 262 Oe and 3600 Oe.

FePt alloys exhibit order-disorder phenomenon. The ordered phase crystallizes in the tetragonal structure and is magnetically hard, while the disordered phase is cubic and magnetically soft. We have exploited this feature and have shown, for the first time, the co-existence of cubic and tetragonal phases, thus giving rise to exchange-coupled spring magnets.

The tensile strength of the alloy specimen is $\sim 50,000$ psi, the highest value among permanent magnets.

- (2) $\text{MnBi}_{1-x}\text{R}_x$ ($\text{R} = \text{Nd}, \text{Dy}$) specimens were prepared to examine the influence of R on the magnetic properties of MnBi. Nearly 30% R could be substituted for Bi. Samples prepared under similar conditions showed that the coercivity of the specimens at room temperature increases from 0.6 kOe for MnBi to ~ 6.4 kOe and ~ 7.8 kOe for Nd and Dy, respectively. Further, the coercivity of the low temperature phase of MnBi increases to a peak value of 25.8 kOe at 280 C.
- (3) Alloys with the composition $\text{RCo}_{7-x}\text{Zr}_x$ were investigated with $\text{R} = \text{Y}, \text{Gd}, \text{Nd}$ or Ho and $x = 0$ to 0.8 . Nearly single-phase materials were obtained with $x = 0.1$ and 0.2 . They stabilize in the TbCu_7 -type structure. Nd and Ho additions significantly modify the magnetocrystalline anisotropy behavior in these systems.
- (4) Band structure calculations on $\text{Fe}(\text{Co})\text{Pt}$ systems were performed.
- (5) Six publications have resulted from this work.
- (6) Details of the above work are described in this report.

ACKNOWLEDGMENT

The following individuals have made significant contributions in the performance of this work: Vijay Chandhok, Mei Qing Huang, Dick Obermyer, Shibaji Saha, C.J. Thong, Brian Zande, Carl Lovejoy, Mike McHenry (Carnegie Mellon University, Subcontractor), Fred Rothwarf (Consultant), Ed Wallace (CMU, Subcontractor) and Joe Horton (Oak Ridge National Laboratory, Subcontractor).

REFERENCES

- (1) K. Watanabe, Materials Transactions, Jpn. Inst. Met, **32**, No. 3, 292-298 (1991).
- (2) E.F. Kneller and R. Hawig, IEEE Trans **MAG 27**, 3588 (1991) and
E. Bruck, Q.F. Xiao, P.D. Thang, M.J. Toonen, F.R. de Boer and K.H.J. Buschow,
Physica B, **300**, 215-229 (2001).
- (3) J.M. MacLaren, D.D. Vvdensky, R.C. Albers and J.B. Pendry, Comput. Phys. Comm.,
60, 365 (1990).
- (4) R.M. Bozorth, "Ferromagnetism", Van Nostrand, Princeton (1978).
- (5) X. Guo, X. Chen. Z. Altounian and J.O. Strom-Olsen, J. Appl. Phys., **73**, 6275 (1993).
- (6) M.Q. Huang, M. Drennan, W.E. Wallace, M.E. McHenry, Q. Chen and B.M. Ma, J. Appl.
Phys., **85**, 5663 (1999).
- (7) Report presented by (the late) Marlin Walmer at the AMPS Review Meetings.
- (8) M.Q. Huang, W.E. Wallace, S. Simizu, A.T. Pedziawiatr, R.T. Obermyer and
S.G. Sankar, J. Appl. Phys., **75**, 6574-76 (1994).

PUBLICATIONS

Results obtained during this study were published in the following articles. Copies of the reprints (pre-print) are attached with this report.

1. "Magnetic and mechanical properties of (Fe,Co)-Pt bulk alloys prepared through various processing techniques",
S. Saha, C.J. Thong, M.Q. Huang, R.T. Obermyer, B.J. Zande, V.K. Chandhok,
S. Simizu and S.G. Sankar,
J. Appl. Phys., **91**, 8810 (2002).

2. "First principles calculations of the electronic structure of $\text{Fe}_{1-x}\text{Co}_x\text{Pt}$ ",
J. M. MacLaren, S.D. Willoughby, M.E. McHenry, B. Ramalingam and S.G. Sankar,
IEEE Trans., **MAG37**, 1277-79 (2001).

3. "Exchange Coupling in FePt Permanent Magnets",
S. Simizu, R. T. Obermyer, B. Zande, V. K. Chandhok, A. Margolin and S. G. Sankar,
J. Appl. Phys., Accepted for publication (To appear in May 2003).

4. "Magnetic properties of $\text{MnBi}_{1-x}\text{R}_x$ (R= rare earth) systems",
S. Saha, M.Q. Huang, C.J. Thong, B.J. Zande, V.K. Chandhok, S. Simizu,
R.T. Obermyer and W.E. Wallace,
ibid., **87**, 6040-42 (2000).

5. "Magnetic properties of the low temperature phase of MnBi",
S. Saha, R.T. Obermyer, B.J. Zande, V.K. Chandhok, S. Simizu, S.G. Sankar and
J.A. Horton,
Ibid., **91**, 8525-27, 2002).

6. "Structure and magnetic properties of $\text{RCo}_{7-x}\text{Zr}_x$ (R= Y, Gd, Nd or Ho and
 $x=0$ to 0.8)",
M.Q. Huang, S.G. Sankar, W.E. Wallace, M.E. McHenry, Q. Chen and B.M. Ma,
Ibid., **87**, 5305-07 (2000).

Magnetic and mechanical properties of (Fe, Co)–Pt bulk alloys prepared through various processing techniques

S. Saha, C. J. Thong, M. Q. Huang, R. T. Obermyer, B. J. Zande, V. K. Chandhok, S. Simizu, and S. G. Sankar^{a)}
Advanced Materials Corporation, 700 Technology Drive, P. O. Box 2950, Pittsburgh, Pennsylvania 15230-2950

Magnetic and mechanical properties of $\text{Fe}_{60}\text{Pt}_{40}$, $\text{Fe}_{60.5}\text{Pt}_{39.5}$ and $(\text{Fe}_{1-x}\text{Co}_x)_{60.5}\text{Pt}_{39.5}$ bulk alloys prepared by a number of processing techniques have been examined. Processing techniques include induction melting, mechanical milling (at ~ 77 K), hot and cold work, and melt extraction. Magnetic properties were determined in the temperature range from 300 to 1100 K using a vibrating sample magnetometer. Melt extracted $\text{Fe}_{60.5}\text{Pt}_{39.5}$ sample appeared to be fully dense and the magnetic properties found to be $4\pi M_s$ (at 1.5 T) ~ 1.08 T, $H_c \sim 270.6$ kA/m, and $(BH)_{\max} \sim 55.7$ kJ/m³. Freezer milled $\text{Fe}_{60.5}\text{Pt}_{39.5}$ sample (loose powder) showed a saturation induction of 1.33 T, and coercivity of 270.6 kA/m at room temperature. Curie temperature for this sample is found to be 450 °C. For the $\text{Fe}_{45.37}\text{Co}_{15.13}\text{Pt}_{39.5}$ (loose powder) sample, coercivity increases to 318 kA/m and the Curie temperature increases to 540 °C. Tensile strength was measured for selected samples. It is found that Fe–Pt and (Fe,Co)–Pt magnets are about 5–10 times mechanically stronger than the rare earth based permanent magnets. Preliminary examination of the structural and magnetic properties of these alloys indicates that the (Fe,Co)–Pt bulk alloys are an excellent system to explore exchange coupling mechanism in permanent magnets. © 2002 American Institute of Physics. [DOI: 10.1063/1.1453327]

I. INTRODUCTION

Fe(Co)–Pt alloys exhibit remarkable structural and magnetic properties.^{1,2} The $L1_0$ phase exhibits high magnetocrystalline anisotropy energy ($\sim 7 \times 10^6$ J/m³), which is comparable to that of SmCo_5 . MacLaren *et al.*³ have recently reported the electronic structure from first principle calculations of this phase. In the early 1980s, Watanabe and Masumoto⁴ reported remarkable permanent magnetic properties of bulk FePt with composition slightly rich in Fe in the $L1_0$ phase. Magnetic properties and microstructures were studied recently on Fe-rich compositions.⁵ Studies on Fe–Pt permanent magnets in thin film form have shown very interesting results, where an energy product as large as 318 kJ/m³ was obtained by inter-grain exchange coupling.^{6,7} In bulk form, the best values⁴ are limited to an energy product of 159 kJ/m³ with remanence of 1.0 T and a coercivity in the range of 240–400 kA/m. The Curie temperature of equiatomic Fe–Pt magnet is around 480 °C. In order to achieve improved properties in bulk magnets, there is a need to elucidate the mechanism of the coercivity in Fe–Pt magnets and to develop practical fabrication methods. Although Fe-rich alloy gives better magnetic properties, the Curie temperature decreases when Fe concentration increases from 50%. Addition of Co in partial replacement of Fe increases the Curie temperature. Compared with rare earth based magnets, Fe–Pt

magnets are ductile and exhibit higher mechanical strength. In this study, we explored various processing techniques to prepare $\text{Fe}_{60}\text{Pt}_{40}$, $\text{Fe}_{60.5}\text{Pt}_{39.5}$ and $(\text{Fe}_{1-x}\text{Co}_x)_{60.5}\text{Pt}_{39.5}$ alloys and examined their structural, magnetic, and mechanical properties.

II. EXPERIMENT

$\text{Fe}_{1-x}\text{Pt}_x$ ($x=39.5, 40.0$) and $(\text{Fe}_{1-x}\text{Co}_x)_{60.5}\text{Pt}_{39.5}$ ($y=0.0, 0.25, 0.5, 0.75, 1.0$) alloys were prepared by rf induc-

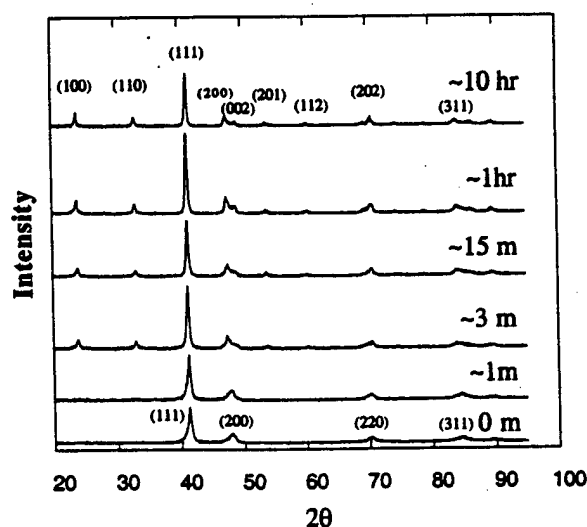


FIG. 1. X-ray diffraction of low temperature milled $\text{Fe}_{60.5}\text{Pt}_{39.5}$ powder samples after annealing at 600 °C for different duration of time.

^{a)}Electronic mail: sgsankar1224@yahoo.com

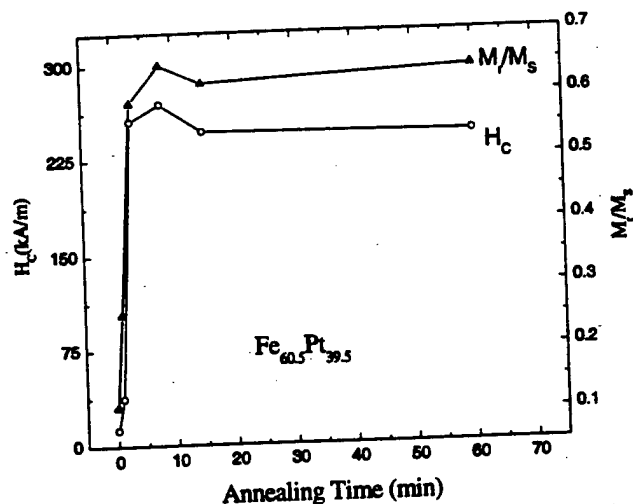


FIG. 2. Coercivity and remanence ratio of $\text{Fe}_{60.5}\text{Pt}_{39.5}$ at room temperature as a function of annealing time; annealing was done at 600°C .

tion melting of the stoichiometric quantities of the metals in an alumina crucible. The purities of all the starting metals were 99.95%. After casting, four different techniques were employed to process the samples: (1) shaped into rectangular specimens and homogenized at 1325°C for about 1 h, quenched in ice water, and subsequently annealed typically at 600°C for 10 h in a sealed tube with partial argon atmosphere; (2) mechanically chipped and pulverized in a freezer mill at 77 K to form fine powder, and then heat treated at $\sim 600^\circ\text{C}$ for 0–10 h; (3) hot and cold worked the as-cast alloy; (4) extracted from melt in a 2–3 mm-diam quartz tube and homogenized at 1200°C for 1 h, quenched in chilled water, and subsequently annealed at 600°C for 10 h in a sealed Vycor tube with partial argon atmosphere.⁴ For annealing, the samples were always inserted into the furnace when the appropriate temperature was reached and taken out promptly after a predetermined time. Samples were characterized using an x-ray diffractometer. Magnetic properties were studied using a vibrating sample magnetometer, and an hysteresis loop tracer. Tensile strength of the samples was

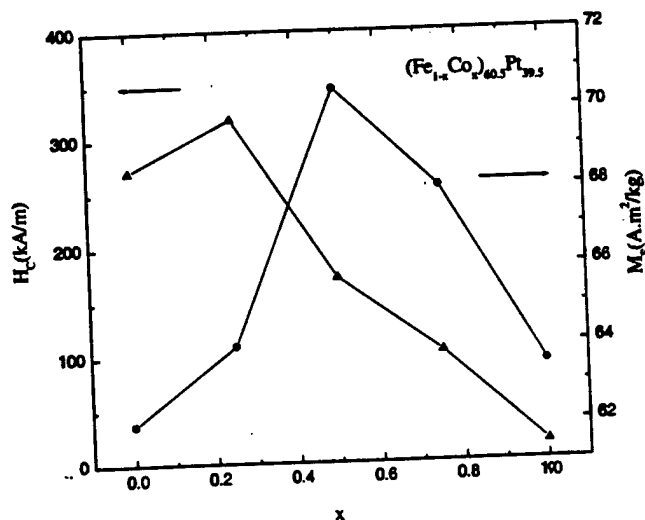


FIG. 3. Coercivity and saturation magnetization of $(\text{Fe}_{1-x}\text{Co}_x)_{60.5}\text{Pt}_{39.5}$ at room temperature as a function of Co concentration.

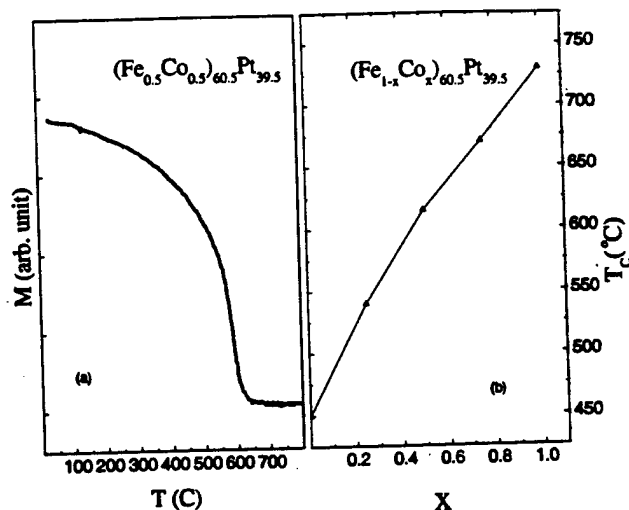


FIG. 4. (a) Temperature dependent magnetization of $(\text{Fe}_{0.75}\text{Co}_{0.25})_{60.5}\text{Pt}_{39.5}$. (b) Variation of T_c as a function of Co concentration.

determined by converting Brinnel hardness number measured on each sample.

III. RESULTS AND DISCUSSION

The low temperature milled $\text{Fe}_{60.5}\text{Pt}_{39.5}$ samples were heat treated at 600°C for different time durations to obtain the fct phase. X-ray diffraction was performed after each heat treatment to detect the structural change. A typical set of results is shown in Fig. 1. The fct phase begins to appear when the sample is exposed to 600°C for ~ 3 min and its concentration increases with increased time of heat treatment at 600°C . Field dependent magnetization was studied for all the $\text{Fe}_{60.5}\text{Pt}_{39.5}$ powder samples heat treated for different time durations. The coercivity and remanence ratio are plotted in Fig. 2 as a function of annealing time. The coercivity and remanence ratio increase rapidly as the time of annealing increases, reaching maximum values of 271 kA/m and 0.6, respectively, for the annealing time of 8 min. A saturation induction of 1.33 T was achieved in this sample. As the sample is annealed longer than 8 min, coercivity starts to deteriorate. This is probably due to the grain growth.

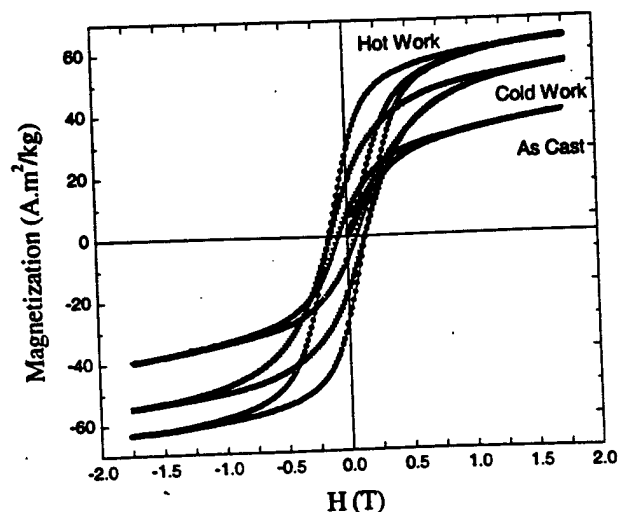


FIG. 5. M - H curves of the hot and cold worked $\text{Fe}_{60.5}\text{Pt}_{39.5}$ alloy.

TABLE I. Magnetic properties of the hot and cold worked $\text{Fe}_{60.5}\text{Pt}_{39.5}$ samples.

	M_r A m ² /kg	M_{\max} (at 1.75 T) A m ² /kg	H_c kA/m
As cast	7	40	56
Cold work	15	55	80
Hot work	30	64	120

Figure 3 shows the coercivity and the saturation magnetization of the $(\text{Fe}_{1-x}\text{Co}_x)_{60.5}\text{Pt}_{39.5}$ samples as Co content is increased. The coercivity generally decreases as the content of Co increases. Because addition of Co tends to stabilize the fcc phase at a given composition, the decrease in coercivity with the increase in Co content is expected. However, for $x=0.25$, the coercivity shows a slight increase. This point needs further examination. Figure 3 also shows that saturation magnetization increases with Co concentration, reaches maximum for $x=0.5$ (30.25 at. %) and then decreases for higher concentration. This behavior is reminiscent of the classic Fe-Co binary alloy (Slater-Pauling curve) where the maximum moment is achieved for about 35 at. % Co.⁸

Temperature dependent magnetization was measured on the $(\text{Fe}_{1-x}\text{Co}_x)_{60.5}\text{Pt}_{39.5}$ system to study the effect of Co concentration on the Curie temperature. Figure 4(a) shows representative data on the sample with $x=0.50$, for which the T_C is 615 °C. Figure 4(b) shows the variation of T_C with Co content. Considering the changes in the magnetic properties such as coercivity, saturation magnetization, and remanence, Co concentration of about 15.1 at. % seems to be the most appropriate for applications where high operating temperature is required.

Plastic deformation processes such as cold and hot work were used to enhance the magnetic properties of the as-cast $\text{Fe}_{60.5}\text{Pt}_{39.5}$ alloy. Figure 5 shows the M - H curves (open loop measurement and not corrected for demagnetization) of cold and hot worked samples. Table I shows the magnetization, remanence, and coercivity data. It is clearly seen that me-

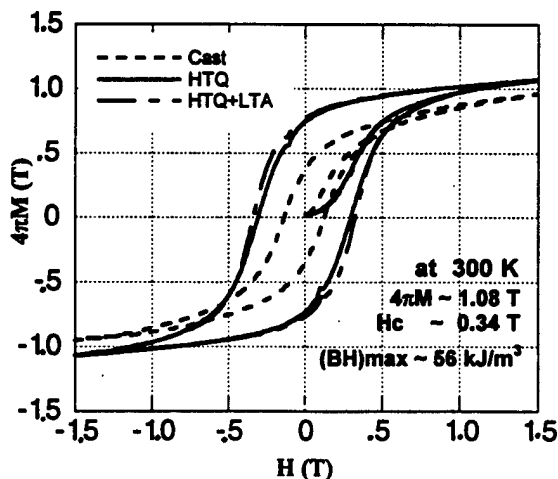
FIG. 6. The $4\pi M$ vs H of melt extracted $\text{Fe}_{60.5}\text{Pt}_{39.5}$ alloy. HTQ: quenched from 1325 °C. LTA: annealing done at 600 °C.

TABLE II. Mechanical properties Fe-Pt and Fe-Co-Pt. BHN: Brinell hardness number.

Sample	Mechanical strength	
	BHN(1/16 in. ball)	Tensile strength (psi)
$\text{Fe}_{60}\text{Pt}_{40}$	97	47 900
$\text{Fe}_{60.5}\text{Pt}_{39.5}$	108	53 300
$(\text{Fe}_{0.5}\text{Co}_{0.5})_{60.5}\text{Pt}_{39.5}$	86	42 600
SmCo_5		6000
$\text{Nd}_2\text{Fe}_{14}\text{B}$		11 000

chanical work improves the magnetic properties. Hot working is found to be more effective in improving the magnetic properties than the cold working. However, the casting method itself provides important implications.

Improved magnetic properties were found in $\text{Fe}_{60.5}\text{Pt}_{39.5}$ samples prepared by melt extraction method where the melt was sucked into a quartz tube and later quenched from 1200 °C into water and then was annealed for 10 h at 600 °C. M - H data (open loop measurement and not corrected for demagnetization) on the melt extracted sample are shown in Fig. 6. The remanence and coercivity of melt extracted sample (after heat treatment) are 41 A m²/kg and 271 kA/m, respectively. These values are higher than the corresponding values for the hot worked sample, viz., 30 A m² and 119 kA/m, respectively (see Fig. 5). Further, the ratio of remanent magnetization to the saturation magnetization for the melt extracted sample as well as the freezer-milled samples (see Figs. 6 and 2) is >0.6 . This value is 0.5 for isotropic magnets. The enhancement of this ratio observed by us indicates the development of texture or exchange coupling between the fcc and the fct phases. Further experiments are in progress to ascertain this mechanism.

Brinell hardness number was determined using stainless steel balls of 1/16 in. diameter for the Fe-Pt and Fe-Co-Pt samples. For each sample, data were taken from an average of five measurements. Tensile strength was calculated from the averaged Brinell hardness number. The results are displayed in Table II along with the published values on SmCo_5 and $\text{Nd}_2\text{Fe}_{14}\text{B}$ magnets. It may be noted that Fe-Pt and Fe-Co-Pt magnets are about 5–10 times mechanically stronger than the rare earth based permanent magnets.

ACKNOWLEDGMENTS

This work was supported by DARPA through the Office of Naval Research under Contract No. N14-98-C-0268 and through the Army Research Office under Contract No. DAAD 19-01-1-0546.

¹L. Graf and A. Kussmann, Z. Phys. 36, 544 (1935).

²O. A. Ivanov, L. V. Solina, V. A. Demshina, and L. M. Megat, Phys. Met. Metallogr. 35, 81 (1973).

³J. M. MacLaren, S. D. Willoughby, M. E. McHenry, B. Ramalingam, and S. G. Sankar, IEEE Trans. Magn. 37, 1277 (2001).

⁴K. Watanabe and H. Masumoto, Trans. Jpn. Inst. Met. 24, 627 (1983).

⁵Y. Tanaka, N. Kimura, K. Hono, K. Yasuda, and T. Sakurai, J. Magn. Mater. 170, 289 (1997).

⁶M. Watanabe and M. Homma, Jpn. J. Appl. Phys., Part 2 35, L1264 (1996).

⁷J. P. Liu, C. P. Luo, Y. Liu, and D. J. Sellmyer, Appl. Phys. Lett. 72, 483 (1998).

⁸R. M. Bozorth, Ferromagnetism (IEEE, NY, 1993), p. 195.

First Principles Calculations of the Electronic Structure of $\text{Fe}_{1-x}\text{Co}_x\text{Pt}$

J. M. MacLaren, S. D. Willoughby, M. E. McHenry, B. Ramalingam, and S. G. Sankar

Abstract—The L_{10} alloys CoPt and FePt have strong uniaxial magneto-crystalline anisotropy as a consequence of the layering of Co or Fe and Pt planes. This makes these compounds of interest in permanent magnet applications. In this work we present the results of a study of the magnetic properties of the L_{10} alloys $\text{Fe}_{1-x}\text{Co}_x\text{Pt}$ for the range of compositions from FePt to CoPt . Local spin density calculations using the coherent potential approximation are used to follow trends in the magneto-crystalline anisotropy and magnetic moments across the composition range. Total energy calculations of ordered and disordered alloys are used to develop a pseudo-binary phase diagram of the Fe/Co layer predicting regions of phase separation in this layer at temperatures below 650°C .

Index Terms—Binary phase diagram, coherent potential approximation, local spin density calculations, magneto-crystalline anisotropy.

I. INTRODUCTION

THE L_{10} $\text{Fe}_{1-x}\text{Co}_x\text{Pt}$ alloys have technologically important magnetic properties. In particular the large uniaxial magneto-crystalline anisotropy that results from the intrinsic layering of the crystal is desirable for potential permanent magnet applications. The L_{10} structure is a natural superlattice and just like many of the artificially grown superlattices the interfaces produce a large uniaxial anisotropy. In the paper we will study the electronic and magnetic properties of $\text{Fe}_{1-x}\text{Co}_x\text{Pt}$ alloys using first principles local spin density electronic structure calculations. The alloys are assumed to have a substitutionally disordered Fe/Co plane. The technique used in our study is the layer Korringa Kohn Rostoker method (LKRR) [1]. The disorder is treated within the coherent potential approximation [2]. This approach has been used previously to calculate the electronic structure of disordered magnetic alloys [3]. One benefit of the method is that it is able to handle both ordered and disorder compounds within the same set of approximations which facilitates a comparison of trends. The lattice parameters (a , and c/a) as a function of composition were taken from published experiment data [4].

Manuscript received October 13, 2000.

This work was supported by the National Science Foundation, under Grant Award DMR-9971573, and by DARPA under award DARPA Grant MDA 972-97-1-003, and through the Office of Naval Research under Contract N14-98-C-0268.

J. M. MacLaren and S. D. Willoughby are with the Department of Physics, Tulane University, New Orleans, LA 70018 USA (e-mail: {macLaren; swillou}@tulane.edu).

M. E. McHenry and B. Ramalingam are with the Department of Materials Science and Engineering, Carnegie Mellon University, Pittsburgh, PA 15213 USA (e-mail: {mm7g; bmk}@andrew.cmu.edu).

S. G. Sankar is with Advanced Materials Corporation, Pittsburgh, PA 15230 USA (e-mail: sankar@advanced-material.com).

Publisher Item Identifier S 0018-9464(01)05608-4.

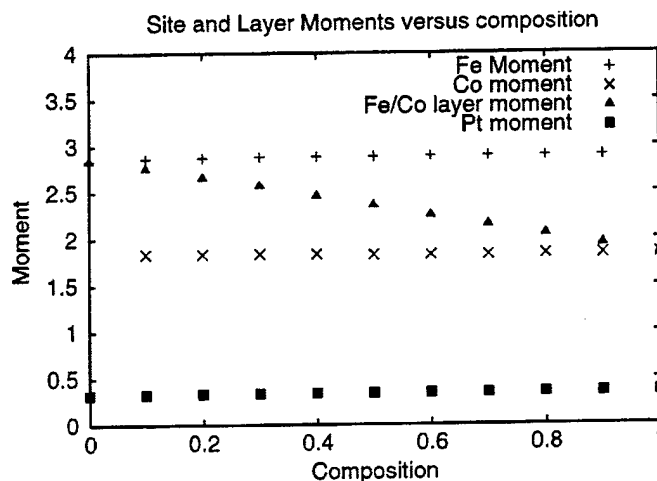


Fig. 1. Site moments for Fe, Co, and Pt as a function of the alloy composition. $x = 0$ corresponds to FePt and $x = 1$ to CoPt .

II. RESULTS

In the first part of this work, we have focused on the variation of magnetic moments as a function of composition. The individual site moments for Fe, Co, and Pt, as well as the composition weighted Fe/Co layer moments are shown in Fig. 1. The magnetizations for FePt and CoPt compare favorably to measured values. We find for FePt a magnetization of 1170 emu/cm^3 with a measured magnetization of 1140 emu/cm^3 [5], while for CoPt calculated and measured values are 750 emu/cm^3 and 800 emu/cm^3 [6] respectively. The Co and Fe moments in the $\text{Fe}_{1-x}\text{Co}_x\text{Pt}$ alloy have enhanced local moments as compared with elemental Co and Fe. BCC Fe has a moment of about $2.2 \mu_B$ while the Fe moment in the L_{10} alloy lies between 2.8 and $2.9 \mu_B$. The enhancement of the Co site moment is not so dramatic, showing an increase from about $1.6 \mu_B$ for HCP Co to around $1.8 \mu_B$ in the alloy. Going from FePt to CoPt we find a slow increase in the Fe moment while the Co site moment is approximately constant. The variation in the Fe moment is consistent with typical behavior of Fe as a function of the effective number of Fe neighbors. The moment at an Fe surface has been predicted to be as large as $3 \mu_B$ [7]. Pt, while nonmagnetic is readily polarized when in proximity to a ferromagnetic atom and a moment of about $0.3 \mu_B$ is induced by the ferromagnetic Fe/Co layer. Since the Fe and Co moments are roughly independent of composition, we see a reasonably linear variation in the layer moment with composition, and it follows a simple rule of mixtures.

The spin resolved densities of states for the Fe, Co, and Pt atoms, not shown due to space limitations, in the alloy show

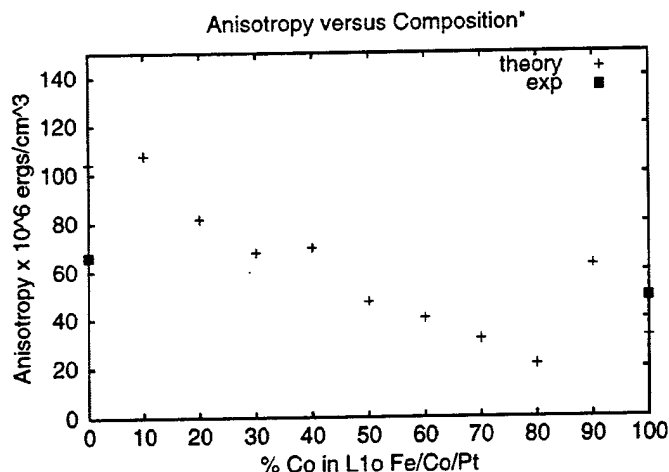


Fig. 2. Uniaxial anisotropy constant K_1 as a function of the percentage of Co in the alloy. Experimental data for the two ordered $L1_0$ alloys are marked by the filled boxes.

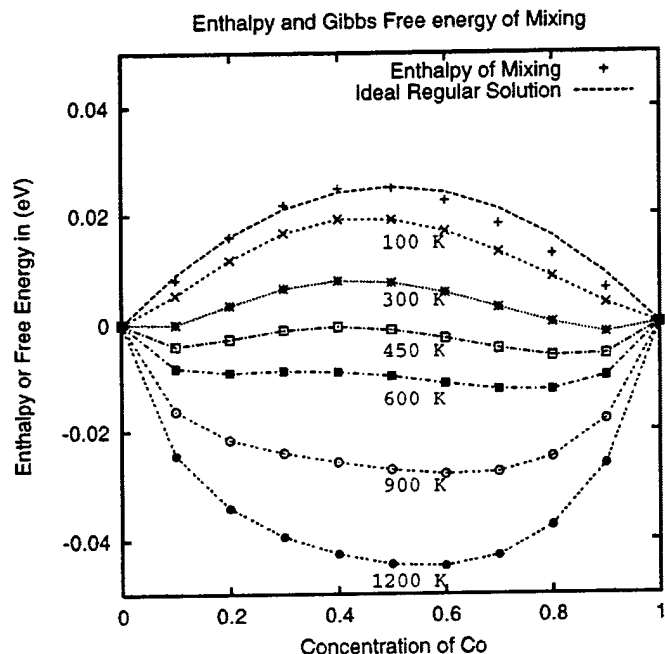


Fig. 3. Comparison of enthalpy of mixing obtained from first principles calculations compared with predictions of the ideal regular solution. Calculated Gibbs Free energy curves at various temperatures as function of alloy composition.

an almost completely filled majority spin band. Hybridization between minority Pt and minority Fe and Co states broadens the Pt d-band by about 2 eV, and the Fermi energy passes through a local minimum. The alloy exhibits strong ferromagnetism with the Fermi energy states primarily of minority spin character.

The magneto-crystalline anisotropy as a function of alloy composition is shown in Fig. 2. The anisotropy calculations were based upon the force theorem [8] in which the anisotropy energy, defined as the difference in total energy between systems with two different magnetization directions—easy and hard—is found using self-consistent potentials that did not include spin-orbit coupling. The force theorem connects the total energy difference to the difference in the one electron energy

once spin-orbit coupling is included provided the same potential is used for both magnetization directions. Test calculations that included spin-orbit coupling in the self-consistent step results in anisotropies that differ by about 10%, consistent with our earlier experience [9]. The experimental results for the uniaxial anisotropy constant K_1 for CoPt, 49×10^6 ergs/cm³ [6], and FePt, 66×10^6 ergs/cm³ [5] are in reasonable agreement with our calculated values. Two possible origins of discrepancy are disorder on the Pt sublattice and choice of lattice constant. Calculations have shown that the anisotropy is quite sensitive to the a lattice constant. While the variation is on the whole monatomic, there are slight peaks in anisotropy close to the FePt and CoPt ends of the graph.

Previous work using the nearest neighbor Neel model [10] to describe the anisotropy of this alloy predicts a smooth change in anisotropy as a function of composition [11]. In previous studies the variation in anisotropy for Co/Pd and Co/Pt superlattices has been quantitatively described by this model [9]. In comparing predictions of the Neel model to those of more detailed electronic structure calculations it was observed that the Neel model described trends on the average rather than any one particular system, and that there could be significant scatter between first principles work and the Neel model. This is not too surprising since the Neel picture, parameterized in terms of effective pair interactions, does not include subtle changes associated with specifics of the electronic structure. Nonetheless the model has use and in this system would show the overall trends in alloying.

The final part of this paper describes our use of first principles calculations in a study of the pseudo-binary phase diagram of the Fe/Co plane. Our total energy calculations show that Fe and Co obey a pseudo-binary regular solution model, predicting phase separation (in {100} planes) at low temperatures, and random mixing above 650 °C. The calculated total energies for the $\text{Fe}_{1-x}\text{Co}_x\text{Pt}$ ternary alloys are analyzed here within a quasichemical, Regular Solution Model (RSM) to study the possibility of Fe and Co partitioning. In this model we would write the alloy energy E as

$$E = P_{CC}E_{CC} + P_{FF}E_{FF} + P_{CF}E_{CF}, \quad (1)$$

where P_{CC} , P_{FF} , and P_{CF} , are the probability of finding Co-Co, Fe-Fe, and Co-Fe bonds, respectively, within the {100} plane and E_{CC} , E_{FF} , and E_{CF} , are the energies of these bonds. In order to develop the phase diagram we only need the enthalpy of mixing which we determine from total energy calculations of the alloys as well as the two ordered $L1_0$ compounds FePt and CoPt. We have not extracted effective pair interactions from this data though we intend to investigate this in more detail in future. The change in total energy due to mixing, ΔE_m (enthalpy of mixing, ΔH_m) as follows:

$$\Delta E_m = \Delta H_m = E_{cpa}(\text{alloy}) - (1-x)E(\text{FePt}) - xE(\text{CoPt}), \quad (2)$$

where $E_{cpa}(\text{alloy})$ is the total energy of the disordered alloy found from the LKKR calculations within the coherent potential approximation, and the other two energies in (2) are the LKKR total energies of the ordered structures.

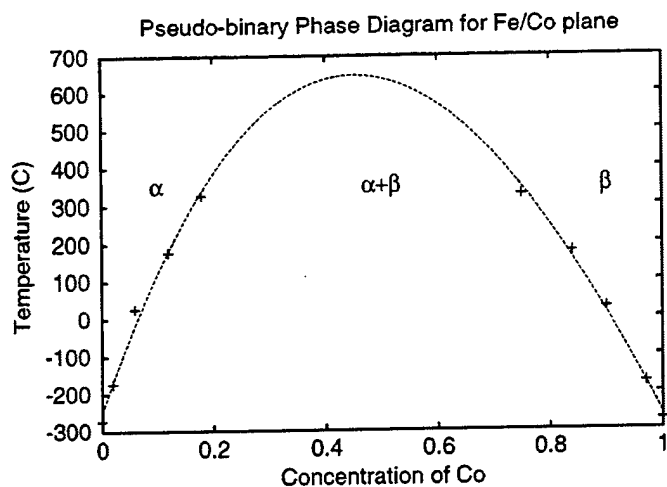


Fig. 4. Pseudo-binary phase diagram for L1_0 $\text{Fe}_{1-x}\text{Co}_x\text{Pt}$ alloys. The curve is a third order polynomial fit through the data.

The thermodynamics of mixing are addressed through examination of the Gibbs free energy of mixing

$$\Delta G_m = \Delta E_m - T\Delta S_m, \quad (3)$$

where we use a simple configurational entropy term ΔS_m given by

$$\Delta S_m = -k_B(x \ln(x) + (1-x) \ln(1-x)). \quad (4)$$

Fig. 3 illustrates the energy (enthalpy) of mixing difference as a function of alloy composition (x) for all of the $\text{Fe}_{1-x}\text{Co}_x\text{Pt}$ ternary alloys studied. This energy difference is seen to deviate only slightly from the $x(1-x)$ dependence predicted for an ideal regular solution. Also shown are Gibbs Free energies of mixing constructed at different temperatures between 100 K and 1200 K, respectively. A common tangent construction can be used to determine points on a pseudo-binary phase diagram for $\text{Fe}_{1-x}\text{Co}_x\text{Pt}$. Fig. 4 illustrates an $\text{Fe}_{1-x}\text{Co}_x\text{Pt}$ pseudo-binary phase diagram constructed from the data of Fig. 3. It can be seen that Fe and Co obeys a pseudo-binary regular solution model predicting phase separation (in $\{100\}$ planes) at low temperatures into a Co rich α -phase and an Fe rich β -phase, respectively.

III. CONCLUSIONS

In this paper we have studied the variation in magnetic properties in the L1_0 alloys $\text{Fe}_{1-x}\text{Co}_x\text{Pt}$ as a function of

composition. The atomic moments are almost constant across the series as a result of strong ferromagnetism, leading to magnetization variations that follow a simple rule of mixtures. The Fe and Co moments are both enhanced over respective bulk values and show behaviors typical of the atoms at interfaces where the number of like coordinating atoms is reduced. The uniaxial anisotropy constant K_1 follows the trends expected by the Neel model, though there some enhancement near the two ordered ends. Total energy calculations of both ordered and disordered alloys have been used to construct a pseudo-binary phase diagram for the Fe/Co layer. The enthalpy of mixing is close to that of the ideal regular solution, and the system shows phase separation below 650 °C.

ACKNOWLEDGMENT

S. Willoughby gratefully acknowledges the support of the CMU DSSC summer exchange program. The Data Storage Systems Center at CMU is supported under a Grant of no. ECD-89-07 068 from National Science Foundation.

REFERENCES

- [1] J. M. MacLaren, D. D. Vvdensky, R. C. Albers, and J. B. Pendry, "Layer Korringa-Kohn-Rostoker electronic structure code for bulk and interface geometries," *Comput. Phys. Comm.*, vol. 60, pp. 365-389, 1990.
- [2] J. M. MacLaren, A. Gonis, and G. Schadler, "First-principles calculation of stacking-fault energies in substitutionally disordered alloys," *Phys. Rev. B*, vol. 45, pp. 14 392-14 395, 1992.
- [3] J. M. MacLaren and R. H. Victora, "Theoretical predictions of interface anisotropy in the presence of interdiffusion (invited)," *J. Appl. Phys.*, vol. 76, pp. 6069-6074, 1994.
- [4] J. C. Wooley and B. Bates, *J. Less Common Metals*, vol. 1, p. 382, 1959.
- [5] J. P. Liu, C. P. Luo, Y. Liu, and D. J. Sellmyer, "High energy products in rapidly annealed nanoscale Fe/Pt multilayers," *Appl. Phys. Lett.*, vol. 72, pp. 483-485, 1998.
- [6] S. H. Liou, Y. Liu, S. S. Malhotra, M. Yu, and D. J. Sellmyer, "Magnetic properties of nanometer-size copt particles," *J. Appl. Phys.*, vol. 79, pp. 5060-5062, 1996.
- [7] C. Li, A. J. Freeman, H. J. F. Jansen, and C. L. Fu, "Magnetic anisotropy in low-dimensional ferromagnetic systems: Fe monolayers on Ag(001), Au(001), and Pd(001) substrates," *Phys. Rev. B*, vol. 42, pp. 5438-5442, 1990.
- [8] A. R. MacKintosh and O. K. Anderson, *Electrons at the Fermi Surface*: Cambridge University Press, 1980.
- [9] R. H. Victora and J. M. MacLaren, "Theory of magnetic interface anisotropy," *Phys. Rev. B*, vol. 47, pp. 11 583-11 586, 1993.
- [10] L. Neel, "Anisotropie magnetique superficielle et surstructures d'orientation," *J. de Physique et le Radium*, vol. 15, pp. 225-239, 1954.
- [11] S. Jeong and M. E. McHenry, *Mat. Res. Soc. Symp. Proc.*, vol. 577, 1999, p. 365.

Exchange Coupling in FePt Permanent Magnets

S. Simizu, R. T. Obermyer, B. Zande, V. K. Chandhok, A. Margolin and S. G. Sankar

Advanced Materials Corporation

Pittsburgh, PA 15219, U. S. A.

Abstract

FePt (for 40 ~ 60 at. % Fe) exhibits an order-disorder transformation. The disordered phase is fcc and magnetically soft while the ordered phase is tetragonal and shows high magnetic anisotropy. Since the volume changes between the two phases are small, it is easy for the soft and hard phases to co-exist in a uniform manner. Thus, we have an ideal system to investigate the basic features of exchange coupled magnets. Bulk $\text{Fe}_{0.6}\text{Pt}_{0.4}$ exhibits reasonably large permanent magnetic properties with a maximum energy product of ~15 MGOe (120 kJ/m^3) without special processes to promote grain alignment. The high energy product is partially a result of the high ratio of remanence to the saturation induction which amounts to 0.68 as opposed to the ratio of 0.5 for an assembly of randomly oriented uniaxial magnets. This enhanced remanence is predicted by the exchange-spring magnet model for a mixture of cubic and uniaxial phases. In order to verify that the high remanence of the FePt magnets is indeed caused by this exchange mechanism and not by fortuitous formation of magnetic texture during sample preparation, we have prepared cubic samples of $\text{Fe}_{0.6}\text{Pt}_{0.4}$ and measured the B-H loops along the three principal directions of the cube using a VSM. The hysteresis loops are

identical in all three directions, indicating absence of strong texture in this material.

After correction of the demagnetizing factor, the ratio of remanence to saturation induction is $0.66 \sim 0.68$. This is consistent with the exchange coupling model. The highest energy product in our study was found for the as-quenched samples. Further annealing, with the intention to promote formation of the hard magnetic phases, reduced the coercivity and remanence. This suggests that improved results may be achieved by initial suppression of the formation of the hard phases by modification of the quenching process and alloying. The ideal exchange coupled system may be designed based on such a starting material.

Introduction

Properties of a composite of magnetically hard and soft materials that are exchange coupled have been a focus of extensive theoretical and experimental investigation ever since Kneller and Hawig¹ proposed making a permanent magnet through a two-phase nanostructure. The interest for such a system arises from a desire to combine two desirable properties, such as a high magnetic saturation of a magnetically soft material and high coercivity of a magnetically hard material, into a single system – a composite magnet. There are severe limitations on the sizes of the soft and hard phases in order to assure a reasonably high nucleation field for the soft phase. Based on theoretical calculations (see, for example, Kneller and Hawig,¹ Skomski and Coey²), it has been shown that the soft material size should be within a few times the Bloch domain wall width (δ_B). Thus, Fe-Pt with $\delta_B \sim 4$ nm [reference 3] has an upper limit for the soft phase of ~ 10 nm. Therefore, a co-mingled structure composed of hard and soft magnetic regions should be used with the soft dimension limited to 2 ~ 3 times the Bloch wall width. Theoretical calculations² indicate the possibility of producing permanent magnets with energy products greater than ~ 90 MGOe (720 kJ/m^3) through the appropriate engineering of structured exchange coupled systems.

One of the basic assumptions of Kneller's enhanced remanence to saturation ratio for exchange coupling is that the hard phase is precipitated in the soft phase matrix. The hard phase is uniaxial while the soft phase may be cubic or uniaxial (hexagonal or tetragonal). For polycrystalline materials with the soft phase having cubic symmetry, the remanence to saturation ratio (m_r) should be approximately 0.68. Under these conditions,

the enhanced remanence to saturation ratio is a strong evidence of realization of such a model system. Of course, when making such a measurement, the tacit assumption is that the enhancement is not the result of some experimental detail such as texturing.

Experimental methods employed to fabricate such composite magnets include melt-spinning,⁵ mechanical alloying,⁶ and deposition techniques. The deposition and melt spinning techniques involve production of amorphous off-stoichiometric compositions in order to precipitate the magnetically soft phase in a magnetically hard matrix. While these experimental results support the basic validity of the concept, the actually achieved magnetic properties have been much lower than those predicted for the ideal case. In view of the difficulty in synthesizing the nanocomposites by starting from nanocrystalline powders, we have attempted to prepare those structures by starting from the bulk alloy and then precipitate out the nanocomposite phase. The appropriate size conditions to promote an ideal exchange coupled system may be realized through heat treatments.

Fe-Pt is an unusually interesting material in this regard. This alloy exhibits an order-disorder transformation near the equiatomic composition. The disordered phase is fcc and magnetically soft while the ordered phase is tetragonal and magnetically hard. Having very similar volumes, these phases readily co-exist in a uniform manner. The hard phase exhibits a large magnetocrystalline anisotropy (7×10^7 erg/cm³ at room temperature) that is comparable to that of SmCo₅. Recently, Sellmyer's group has reported that thin films of Fe-Pt show an energy product of close to 40 MGOe (320 kJ/m³) with coercivities exceeding 40 kOe (3200 kA/m).⁷ Unfortunately, the bulk form

exhibits much lower values, $(BH)_{\max} \sim 20 \text{ MGOe}$ (160 kJ/m^3), $B_r \sim 10 \text{ kG}$ (1.0 T) and $H_c \sim 3 - 5 \text{ kOe}$ ($240 - 400 \text{ kA/m}$).^{8,9,10} One notable result on this system is its high ratio of remanence to the saturation induction which amounts to 0.68. In contrast, this ratio is 0.5 for an assembly of randomly oriented uniaxial magnets. In order to verify that the high remanence of the FePt magnets is indeed caused by the exchange mechanism and not by fortuitous formation of magnetic texture during sample preparation, we have prepared cubic samples of $\text{Fe}_{0.6}\text{Pt}_{0.4}$ and measured the B-H loops along the three principal directions of the cube using a VSM. We have also investigated effects of annealing.

Experimental

$\text{Fe}_{0.6}\text{Pt}_{0.4}$ samples were prepared by RF induction melting of the stoichiometric quantities of the metals in an alumina crucible. The purities of all the starting metals were 99.95 %. Specimens were extracted from the melt in a 2-3 mm diameter quartz tube. The as cast ingots were machined into $\sim 2 \text{ mm}$ cubes and are referred to as the “as cast” samples. Some “as cast” samples were heat treated for 16 hours at either 600°C or 650°C in order to investigate the effects of heat treatment. Hysteresis loops were measured along the three directions of the cubes using a vibrating sample magnetometer (VSM) and remanence, saturation, and coercivity were determined. The measurements along the three directions of the cube enable us to determine if any texturing had occurred during the sample preparation. Demagnetization corrections were made on all measurements and the appropriate magnetic properties were determined. A thermomagnetic analysis (TMA) was performed on an as cast sample to determine the Curie temperature and phase purity.

Results and Discussion

The results of magnetization analysis data on the samples investigated in this study are shown in Table I. Hysteresis loops were obtained in an open loop measurement.

Therefore, it was necessary to make demagnetization corrections to the raw data in order to determine the correct values for the remanence (M_r) to saturation (M_s) ratio. Figure 1 shows the magnetization as a function of applied and corrected (internal) field for an as cast sample of cubic geometry. The M_r/M_s ratio for the corrected data was 0.68, in agreement with Kneller's predicted results for a uniaxial hard magnetic phase precipitated in a cubic soft magnetic matrix. The expected results for a collection of randomly oriented uniaxial magnets would have been 0.50. Therefore, it is clear that the enhanced remanence in the as cast sample is in line with Kneller's exchange coupling model.

Figure 2 shows the room temperature hysteresis loops for the samples as cast and those heat treated for 16 hours at 600 °C and 650 °C. As shown in Fig. 2 and Table I, the maximum values for the remanence, coercivity and energy product occur for the as cast sample. Heat treatment appears to have a negative effect upon these properties. This result is in contrast to that reported by Bruck et al.⁹ who showed that optimum results were obtained after appropriate annealing. It appears that the hard phase has already precipitated out in our samples and subsequent heat treatment just promoted additional conversion of the soft magnetic phase to the hard phase and grain growth of this hard

phase. Thus, it may be possible to improve the results by initial suppression of the formation of the hard phases by modification of the quenching process and alloying.

One could attribute the enhanced remanence to texturing that could occur when the sample was withdrawn from the melt. Figure 3 compares the magnetization curves when the field is applied along the x, y and z axes for the as cast sample. Three curves are nearly identical. As summarized in Table I, the remanence to saturation ratio is virtually the same at ~0.68 for all three directions. This excludes the possibility that certain texturing is responsible for the remanence enhancement. The Curie temperature of the as cast sample was 403 °C, consistent with the value of 330 ~ 400 °C reported by Bruck et al.⁹ for $(\text{Fe}_{0.6}\text{Pt}_{0.4})_{99}\text{Nb}_1$ under varied annealing conditions and comparable with that reported by Watanabe.¹⁰

Acknowledgement

This work was supported by DARPA through the Office of Naval Research under Contract Number N14-98-C-0268 and through the Army Research Office under Contract Number DAAD19-01-1-0546.

References

1. E.F. Kneller and R. Hawig, IEEE Trans **MAG 27**, 3588 (1991).
2. R. Skomski and J.M.D. Coey, Phys. Rev. B, **45**, 15812 (1993).
3. T. Klemmer, D. Hoydick, H.Okumura, B. Zhang and W.A. Soffa, Scripta Metallurgica et Materialia, **33**, 1793(1995).
4. R.F. Sabiryanov and S.S. Jaswal, J. Magn. Magn. Mater., **177-181**, ser. 2, 989-90 (1998).
5. A. Kojima, A. Makino and A. Inoue, Nanostr. Mater., **8**, 1015 (1998).
6. I. Ding, P. G. McCormick and R. Street, J. Magn. Magn. Mater.**124**, 1 (1993).
7. J.P. Liu, C.P. Luo, Y. Liu and D.J. Sellmyer, Appl. Phys. Lett. **72**, 483 (1998).
8. S. Saha, C.J. Thong, M.Q. Huang, R.T. Obermyer, B.J. Zande, V.K. Chandhok, S. Simizu and S.G. Sankar, J.Appl.Phys., **91**, No. 10, 8525-7 (2002).
9. E. Bruck, Q.F. Xiao, P.D. Thang, M.J. Toonen, F.R. de Boer and K.H.J. Buschow, Physica B, **300**, 215-229 (2001).
10. K. Watanabe, Materials Transactions, JIM, **32**, No. 3, 292-298 (1991).

Table I. Energy product, remanence, saturation, remanence to saturation ratio and coercivity of as-cast and heat treated samples

Fe_{0.6}Pt_{0.4}	As Cast			16hrs/600 °C	16hrs/650 °C
	X	Y	Z	Z	Z
BH_{max} (MGOe)	4.87	5.33	5.94	5.36	4.15
B_r (kG)	6.86	7.34	7.63	7.13	6.49
B_s (kG)	10.37	10.92	11.20	10.60	10.36
B_r/B_s	0.66	0.67	0.68	0.67	0.63
H_c (kOe)	2.37	2.34	2.36	2.40	2.11

Figure Captions

Fig. 1. Raw and corrected z-axis magnetization versus magnetizing field for an as cast sample.

Fig. 2. Magnetization versus internal field for as cast and heat treated for 16 hrs at 600 °C and at 650 °C.

Fig. 3. Magnetization versus internal field along the x, y and z axis for the as cast sample and along the z axis for the 600 °C heat treatment sample.

Fig. 1

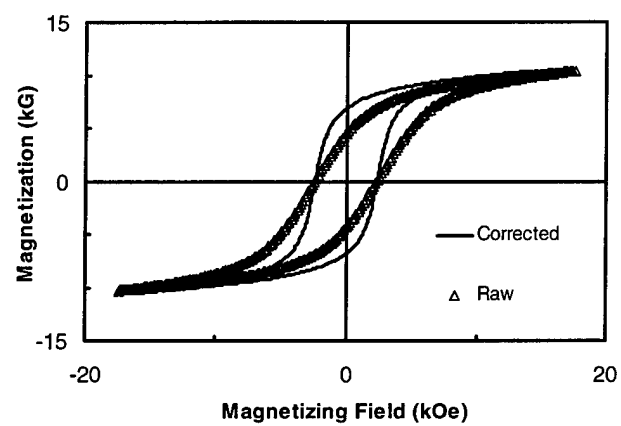


Fig. 2

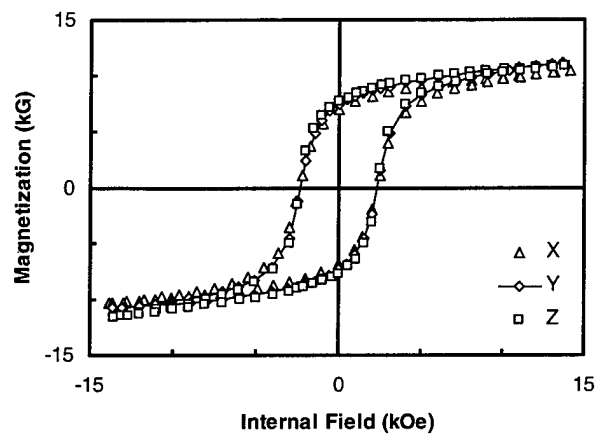
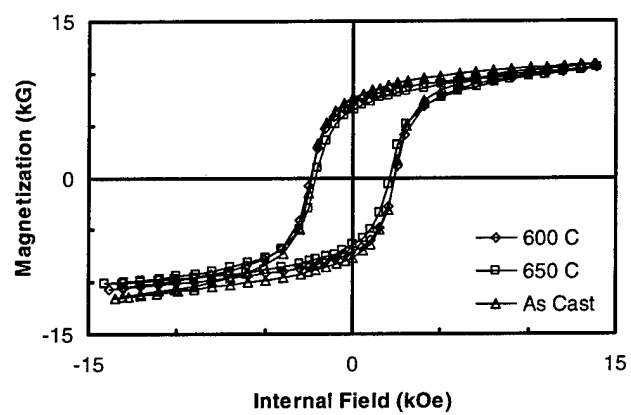


Fig. 3



Magnetic properties of $\text{MnBi}_{1-x}\text{R}_x$ ($\text{R}=\text{rare earth}$) systems

S. Saha, M. Q. Huang, C. J. Thong, B. J. Zande, V. K. Chandhok, S. Simizu, R. T. Obermyer, and S. G. Sankar

Advanced Materials Corporation, 700 Technology Drive, P.O. Box 2950, Pittsburgh, Pennsylvania 15230-2950.

MnBi crystallizes in a NiAs -type hexagonal crystal structure, exhibits a high uniaxial anisotropy, and is potentially useful as a permanent magnet material. We have examined the effect of partial substitution of Bi with rare earth elements on the magnetic properties of MnBi . $\text{MnBi}_{1-x}\text{R}_x$ ($\text{R}=\text{Nd, Dy}$) were prepared by mechanically alloying powders of the constituent elements at liquid nitrogen temperature followed by heat treatment. X-ray diffraction and magnetic measurements were performed on powder samples to characterize the samples. We found that in $\text{MnBi}_{1-x}\text{Nd}_x$, coercivity (at room temperature) increases from 0.7 kOe to 6.6 kOe for $x=0.0$ and 0.3, respectively. In $\text{MnBi}_{1-x}\text{Dy}_x$ the coercivity increases from 0.7 kOe to 7.9 kOe for $x=0.0$ and 0.3. The increase in coercivity may be in part due to the increase in the crystal field anisotropy as Nd or Dy is introduced and in part due to the finer particle size. A magnet made from MnBi shows coercivity of ~ 17 kOe. A very fine particle size is considered to be the reason for this high coercivity. © 2000 American Institute of Physics. [S0021-8979(00)79608-3]

INTRODUCTION

MnBi has received considerable attention¹⁻⁵ for four decades for its unusual magnetic and magneto-optic properties and its potential as a permanent magnet material. It crystallizes in NiAs -type hexagonal crystal structure with the c -axis being the easy direction of magnetization. It exists in several closely related forms,⁶ such as a low-temperature-phase (LTP) which is ferromagnetic and has very high magneto-crystalline anisotropy ($k \approx 10^7$ ergs/cm³); the high-temperature phase (HTP) which is paramagnetic; and the quenched-high-temperature-phase (QHTP), which has very good magneto-optical properties.⁷ It is remarkable that the coercivity of the LTP increases with temperature, exhibits a maximum value of 1.9 T at 277 °C, and has a positive temperature coefficient of coercivity.⁵ Due to these interesting properties, MnBi has a great potential as a permanent magnet material for certain specialized applications. In this paper, we report the effect on the coercivity of the LTP where substitution of Bi by rare earth elements (Nd and Dy) has been examined. A permanent magnet, which shows high coercivity, also has been made from the LTP.

EXPERIMENT

$\text{MnBi}_{1-x}\text{R}_x$ samples were prepared by mechanical alloying powders (~ 44 μm) of the constituent elements in a freezer mill (SPEX 6800). The sample container is a cylindrical polycarbonate tube with stainless steel caps. It has a soft magnetic steel rod inside the tube to provide impact. Powders are loaded in the polycarbonate tube in a glove box (UNILab, Braun) in an inert atmosphere, which contains less than 1 ppm of oxygen. This tube is placed inside two solenoid coils. The coils and the sample tube assembly are then immersed in liquid nitrogen. For all the samples the milling time was 4 h. The samples were then heat-treated for 2 h at 400 °C in argon atmosphere. The process of making LTP MnBi for the purpose of making a magnet is different from

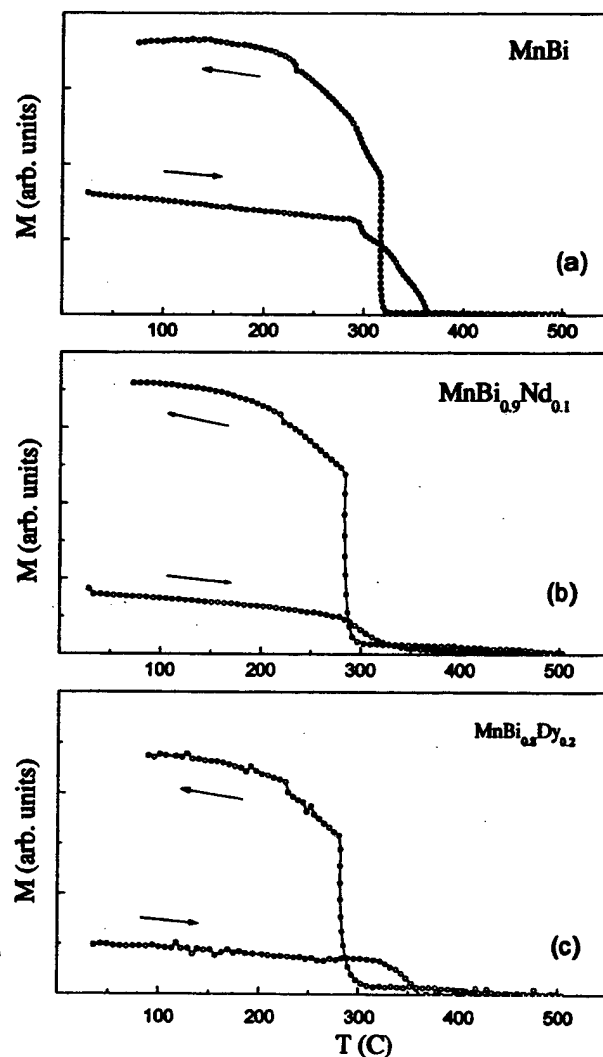


FIG. 1. Magnetization as a function of temperature in an applied field of 500 Oe for (a) MnBi , (b) $\text{MnBi}_{0.9}\text{Nd}_{0.1}$, and (c) $\text{MnBi}_{0.8}\text{Dy}_{0.2}$.

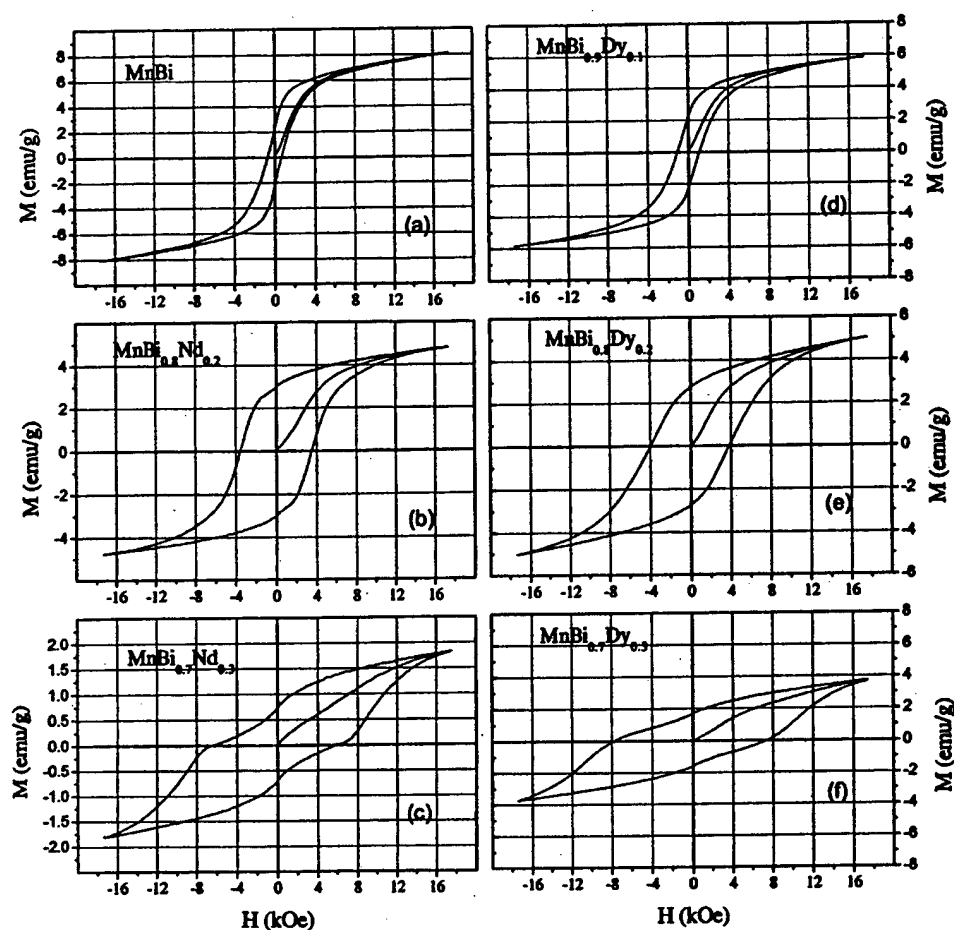


FIG. 2. Hysteresis loops of $\text{MnBi}_{1-x}\text{R}_x$ samples at room temperature.

the rest of the investigation and the procedure is as follows. Mn and Bi powders were mixed in a jar and ball milled for 4 h at room temperature and then heat treated at 440 °C for 2 h. The reacted MnBi was ground and the resulting powder was then ball milled for 24 h. The powder was then sieved (using 38 μm opening) and loaded into a rubber container, then pulse-magnetized and pressed isostatically at 3000 kg/cm^2 .

X-ray diffraction measurements were made at room temperature to characterize the samples using Rigaku diffractometer with $\text{CuK}\alpha$ radiation. Temperature dependent magnetization measurements were made using a vibrating sample magnetometer (EG&G 155) in the temperature range from room temperature to 550 °C in a field of 0.05 T. Field dependent magnetization measurements were performed using a vibrating sample magnetometer (EG&G 4500) at room temperature in a field up to 1.75 T. A SQUID magnetometer (Quantum Design) was used to perform temperature dependent coercivity measurements. A loop tracer (Walker Scientific) was used to perform BH loop measurement on the MnBi permanent magnet.

RESULTS AND DISCUSSION

X-ray diffraction data on $\text{MnBi}_{1-x}\text{R}_x$ samples, after heat treatment, show characteristic intensity peaks of the LTP along with strong peaks due to unreacted Bi. All x-ray data also show a peak which corresponds to Mn indicating some unreacted Mn. Figure 1(a) shows the temperature dependent magnetization on the MnBi sample. The sample is in the

LTP at room temperature and is ferromagnetic. As temperature rises, the magnetic moment shows a precipitous drop and becomes essentially zero at 364 °C. This is in accord with the previous results.² This magnetic transition coincides with structural transformation. The ferromagnetic to paramagnetic transition results because the high temperature phase is paramagnetic. When the sample is cooled from 500 °C, the sample transforms from HTP to the low temperature phase at 317 °C. The transition temperatures were determined by extrapolation. Temperature dependent magnetization measurements have been performed on $\text{MnBi}_{1-x}\text{Nd}_x$ and $\text{MnBi}_{1-x}\text{Dy}_x$ samples. For example, the results on $\text{MnBi}_{0.9}\text{Nd}_{0.1}$ and $\text{MnBi}_{0.2}\text{Dy}_{0.2}$ are shown in Fig. 1(b) and 1(c), respectively. In $\text{MnBi}_{1-x}\text{Nd}_x$ samples the LTP-HTP transition temperatures are 354 °C, 370 °C, and 387 °C for $x=0.1, 0.2$, and 0.3 , respectively. As the Nd concentration increases, the LTP-HTP transition becomes broad. On the other hand, upon cooling, the HTP-LTP transition remains sharp for all Nd concentrations. The HTP-LTP transition decreases to 288 °C, 281 °C, and 280 °C for $x=0.1, 0.2, 0.3$, respectively, compared to 317 °C for MnBi. In $\text{MnBi}_{1-x}\text{Dy}_x$ samples, broadening in the LTP-HTP transition also occurs as Dy concentration increases. The LTP-HTP transition temperatures are 365 °C, 364 °C, and 378 °C for $x=0.1, 0.2$, and 0.3 , respectively. The HTP-LTP transitions remain sharp with a lower transition temperature of 299 °C, 293 °C, 296 °C for $x=0.1, 0.2$, and 0.3 , respectively. In Fig. 1 the increase in the magnetization while cooling compared with

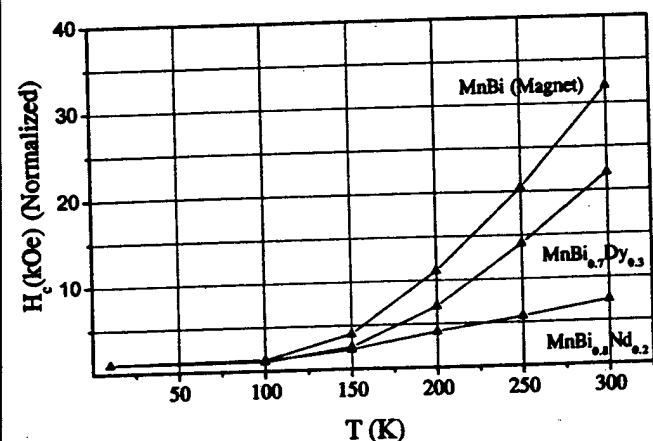


FIG. 3. Temperature dependence of the coercivity, H_c , of $\text{MnBi}_{1-x}\text{R}_x$ samples. The maximum applied field is 55 kOe. The data are normalized at 10 K.

that when heating is most likely due to the formation of more LTP as we passed through the heat treatment temperature on heating cycle.

Figure 2 shows the hysteresis loops on the $\text{MnBi}_{1-x}\text{R}_x$ samples measured at room temperature. The samples are in the LTP. The coercivity of the MnBi sample [Fig. 2(a)] is 0.7 kOe. Figures 2(b) and 2(c) show that substitution of Bi by Nd increases the coercivity; with values 1.4 kOe, 3.6 kOe, and 6.6 kOe for Nd concentration $x=0.1$, 0.2, and 0.3, respectively. A similar increase in the coercivity is observed where Dy [Fig. 2(d), (e), and (f)] is substituted for Bi. The coercivities are 1.0 kOe, 3.9 kOe, and 7.9 kOe for Dy concentration $x=0.1$, 0.2, and 0.3, respectively. The increase in coercivity with the rare earth substitution may be in part due to the increase in the crystal field anisotropy as Nd or Dy is introduced. Fang *et al.*⁸ in their recent study on MnBiR ($\text{R}=\text{Sm}, \text{Dy}$) thin films have reported that the particle size of MnBi alloy films become finer when a small amount of rare earth is introduced. In the present study, the enhancement of the coercivity could also be due to the finer particle size. Saturation magnetization shows an apparent decrease with the addition of either Nd or Dy, however, this may be caused by an increase in the amount of unreacted elements.

The LTP is known to have an anomalous positive temperature dependence of anisotropy energy below and above room temperature. Accordingly, the coercivity also increases with temperature in the LTP. To verify whether this anomalous behavior is affected by rare earth substitution, we conducted coercivity versus temperature measurement on MnBi magnet as well as rare earth substituted $\text{MnBi}_{1-x}\text{R}_x$ powder samples. These results are shown in Fig. 3 where the coercivity is normalized by the value at 10 K. Recently, Guo *et al.*⁹ presented a theory that relates the temperature dependence of anisotropy field and magnetization of MnBi with the observed temperature dependence of the coercivity. The

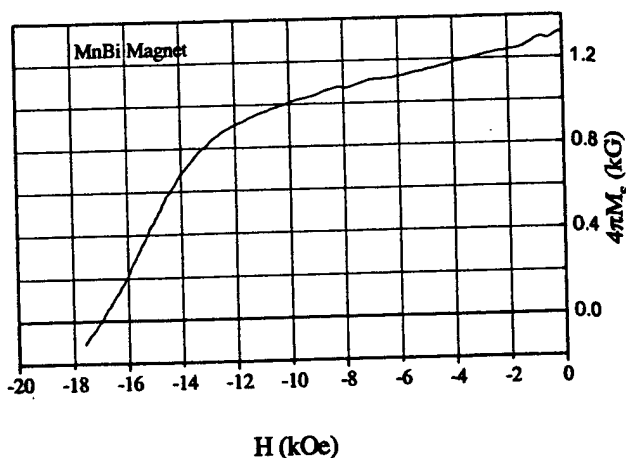


FIG. 4. The second quadrant magnetization curve at room temperature for MnBi magnet.

coercivity of MnBi varies widely depending on the particle size. However, their theory suggests a universal behavior in the temperature dependence of the coercivity. The three curves in Fig. 3 diverge widely, suggesting that the anisotropy field is modified by rare earth substitution.

Figure 4 shows the demagnetization curve for a MnBi magnet. The most important feature of this data is the high coercivity of 16.9 kOe. The saturation induction is 1.55 kG. The maximum coercivity achieved by Guillaud¹⁰ on MnBi magnet was 7 kOe. The significantly higher coercivity achieved in the present study is most likely due to the much finer particle size obtained by extended period of ball milling. The present coercivity value is even higher than 16 kOe achieved by Kishimoto *et al.*¹¹ where an optimum grinding condition was established to achieve maximum coercivity.

ACKNOWLEDGMENTS

This work was supported by DARPA through the Office of Naval Research under Contract No. N14-98-C-0268. The authors thank Professor Mike McHenry (Carnegie Mellon University) for giving permission to use the SQUID magnetometer.

- ¹C. Guillaud, J. Phys. Radium **12**, 492 (1951).
- ²Tu Chen and W. Stutius, IEEE Trans. Magn. **MAG-10**, 581 (1974).
- ³Adams, M. Hubbard, and A. Syeles, J. Appl. Phys. **23**, 1207 (1952).
- ⁴M. Kishimoto and K. Wakai, Jpn. J. Appl. Phys. **14**, 893 (1975).
- ⁵X. Guo, A. Zaluska, Z. Altounian, and J. O. Strom-Olsen, J. Appl. Phys. **69**, 6067 (1991).
- ⁶X. Guo, A. Zaluska, Z. Altounian, and J. O. Strom-Olsen, J. Mater. Res. **5**, 2646 (1990).
- ⁷W. K. Unger, El Wolfgang, H. Harms, and H. Haudek, J. Appl. Phys. **43**, 2875 (1972).
- ⁸Q. Fang, R. Fang, S. Zhang, and D. Dai, J. Magn. Magn. Mater. **188**, 241 (1998).
- ⁹X. Guo, X. Chen, Z. Altounian, and J. O. Strom-Olsen, J. Appl. Phys. **73**, 6275 (1993).
- ¹⁰C. Guillaud, U.S. Patent 2,576,679 (1951).
- ¹¹M. Kishimoto and K. Wakai, Jpn. J. Appl. Phys. **16**, 459 (1977).

Magnetic properties of the low-temperature phase of MnBi

S. Saha, R. T. Obermyer, B. J. Zande, V. K. Chandhok, S. Simizu,
and S. G. Sankar^{a)}

Advanced Materials Corporation, 700 Technology Drive, P.O. Box 2950, Pittsburgh, Pennsylvania 15230

J. A. Horton

Oak Ridge National Laboratory, Oak Ridge, Tennessee 37831

MnBi forms peritectically at $\sim 450^\circ\text{C}$. Preparation of MnBi employing conventional techniques such as arc melting and induction melting results in the segregation of manganese. In order to avoid this segregation, we followed the procedure recommended by Guo *et al.* [X. Guo, A. Zaluska, Z. Altounian, and J. O. Strom-Olsen, *J. Mater. Res.* **5**, 2646 (1990)] and prepared a low-temperature phase of MnBi by melt spinning, followed by heat treatment. Fine powder of MnBi was prepared by ball milling the melt-spun ribbons for various lengths of time. Magnetic properties of these powders were determined. In particular, the temperature dependent coercivity was studied from room temperature to 360°C for the powders ball milled for 2 and 10 h. The coercivity is found to increase with the increase in temperature reaching a maximum of 25.8 kOe at 280°C and then decrease as the temperature is increased further. We also found that a peak in coercivity is observed for the samples milled for 10 h. MnBi shows a first-order transition to a paramagnetic phase at 360°C . In an attempt to increase this transition temperature, an alloy of composition $\text{Mn}_{0.75}\text{Ni}_{0.25}\text{Bi}_{0.5}\text{Sb}_{0.5}$ was made by induction melting. The transition temperature increases from 360°C for MnBi to 400°C for $\text{Mn}_{0.75}\text{Ni}_{0.25}\text{Bi}_{0.5}\text{Sb}_{0.5}$. © 2002 American Institute of Physics. [DOI: 10.1063/1.1450829]

I. INTRODUCTION

MnBi has received considerable attention for its unusual magnetic and magneto-optic properties.^{1–6} It crystallizes in the NiAs-type hexagonal crystal structure with *c* axis as the easy direction of magnetization. It exists in several closely related forms,¹ such as a low-temperature phase (LTP), which is ferromagnetic and has very high magnetocrystalline anisotropy ($K \approx 10^7$ ergs/cm³); the high-temperature phase (HTP), which is paramagnetic; and the quenched-high-temperature phase. It is remarkable that the coercivity of the LTP increases with temperature, exhibits a maximum value of 1.9 T at 277°C , and has a positive temperature coefficient of coercivity.¹ In view of these interesting properties, the LTP of MnBi has very good potential as a permanent magnet material for certain specialized applications. However, due to the segregation of Mn at the peritectic temperature, it is not possible to obtain single-phase LTP MnBi by traditional synthesis techniques. Guo *et al.*⁵ successfully made single-phase MnBi by rapid solidification, followed by annealing. In this article, we report the temperature-dependent coercivity of the LTP of MnBi ball milled for various periods of time. In addition, we also report on the effect of the substitution of manganese and bismuth by nickel and antimony, respectively, on the LTP-HTP transition temperature of MnBi.

II. EXPERIMENT

MnBi samples were prepared by melt spinning equal atomic proportions of Mn (99.99%) and Bi (99.9999%) in an argon atmosphere. The speed of the rotating wheel was 30

m/s and the nozzle diameter of the quartz sample holder was 0.5 mm. The melt was ejected at a pressure of 30 kPa. The collected ribbons were annealed for 30 min. at 400°C in a sealed glass tube under a partial pressure of argon and then slowly cooled to room temperature. The annealed ribbons were then loaded in a jar inside a glove box (<1 ppm O_2) and then ball milled for different durations of time from 1 to 10 h to obtain powder of different particle sizes. Milled powders were collected (inside the glove box) and sieved through a 400 mesh sieve. Magnetization was measured as a function of external field in these samples. Differential scanning calorimetry (Perkin-Elmer DSC7) was used to study the structural transformation of the as-spun ribbons. The as-spun and annealed ribbons were tested using an x-ray diffractometer with Cu $K\alpha$ radiation at room temperature to examine the formation of the LTP. The $\text{Mn}_{0.75}\text{Ni}_{0.25}\text{Bi}_{0.5}\text{Sb}_{0.5}$ sample was made in an induction furnace under an argon atmosphere. The sample was placed in a boron nitride crucible during melting. The sample was cooled by turning off the furnace and by flowing chilled water through the Cu hearth. The sample was then annealed under a partial pressure of argon for 2 h at 440°C . Temperature dependent magnetization measurements were made using a vibrating sample magnetometer in the temperature range from room temperature to 550°C in a field of 0.05 T. Field dependent magnetization measurements at different temperatures were performed using a vibrating sample magnetometer in a field up to 1.75 T.

III. RESULTS AND DISCUSSION

X-ray diffraction data from the as-spun ribbons [Fig. 1(a)] shows the formation of a small fraction of the LTP of MnBi along with signs of unreacted Bi. Figure 1(b) shows

^{a)}Electronic mail: sgsankar1224@yahoo.com

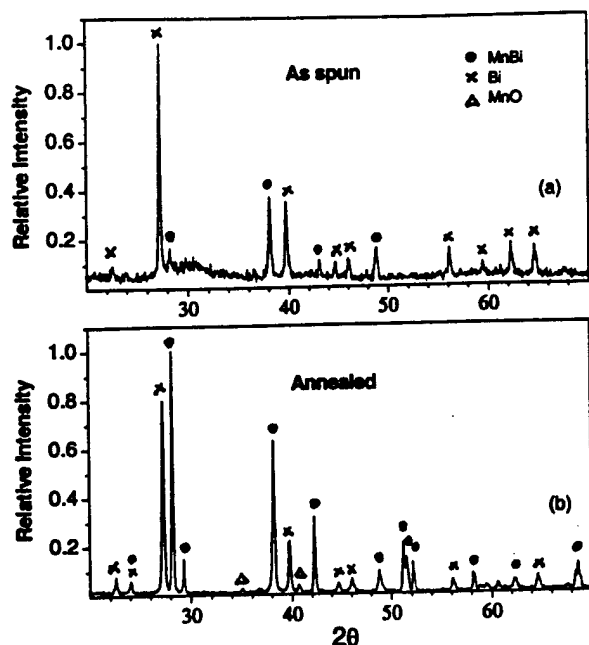


FIG. 1. X-ray diffraction data at room temperature of (a) as-spun MnBi sample and (b) the annealed sample.

the x-ray data obtained from the annealed sample. It clearly indicates the formation of LTP of MnBi during the annealing process by showing a large increase in the characteristic MnBi peaks compared to those found in the as-spun samples.

The formation of the LTP is also evidenced from the differential scanning calorimetry (DSC) data (Fig. 2) obtained from the as-spun sample. The peak in the DSC data depends on the heating rate as has been reported earlier.⁵ A moderate heating rate of 40 °C/min was chosen to clearly see the evidence of formation of the LTP of MnBi. The broad exotherms at around 163 and 219 °C are probably due to the crystallization of some small fraction of ferrimagnetic MnBi phase, and/or metastable Mn₃Bi phase as was suggested by Guo *et al.*¹ from their x-ray diffraction data. The endother-

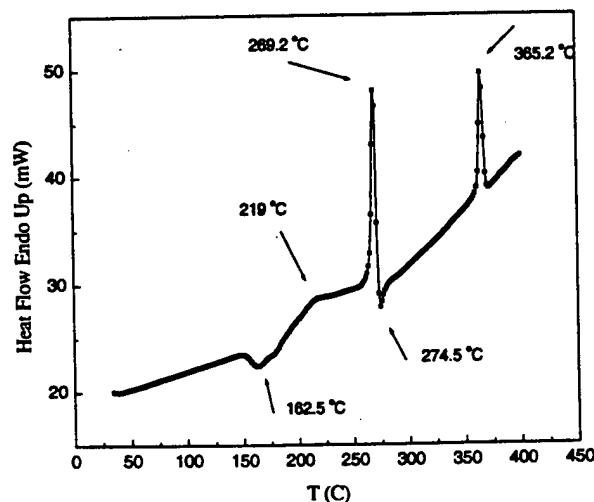


FIG. 2. Differential scanning calorimetry data of as-spun MnBi sample (rate of heating: 40 °C/min).

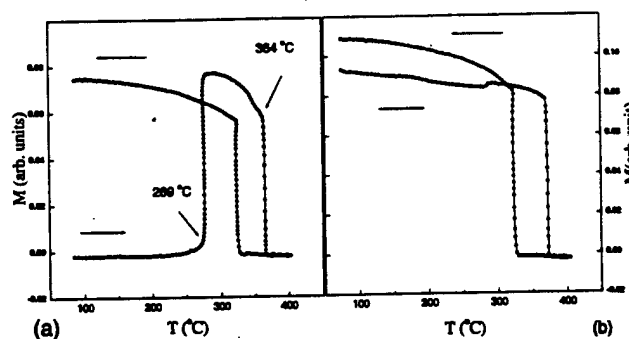


FIG. 3. Magnetization as a function of temperature in an applied field of 500 Oe for (a) as-spun MnBi sample; (b) annealed sample.

mic peak at 269.2 °C shows the characteristic melting temperature of eutectic phase (according to the phase diagram). The next exothermic peak at 274.5 °C is due to the formation of the LTP phase. The LTP-HTP transition is evidenced by the peak at 365.2 °C. A closer look at the temperature-dependent magnetization data [Fig. 3(a)] obtained on the as-spun sample also confirms the explanation of the transitions found in the DSC data. The sharp rise in magnetization at ~269 °C indicates formation of the LTP of MnBi. This transition temperature coincides with the melting temperature of the eutectic phase. At around 364 °C the sample goes through the structural phase transformation into the HTP phase, accompanied by the paramagnetic transition. Figure 3(b) shows the temperature-dependent magnetization on the annealed sample, which indicates that the phase transition is of the first order. The above observations are consistent with the reports published in the literature.^{1,5}

Figure 4 shows the *M* versus *H* data at room temperature from the annealed melt spun sample prior to ball milling. The coercivity is 0.66 kOe. Magnetization versus external field measurement was done on all the samples prepared by ball milling for various periods of time. Figure 5 shows the variation of coercivity with the ball-milling time. It shows that the coercivity increases markedly to 12.5 kOe after 2 h

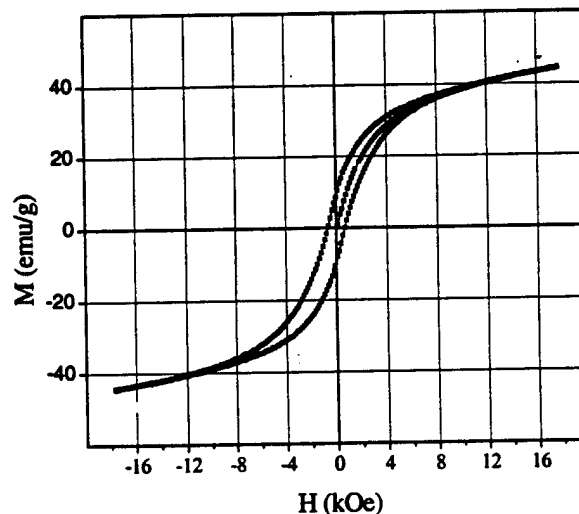


FIG. 4. Magnetization vs external field data at room temperature of the LTP MnBi.

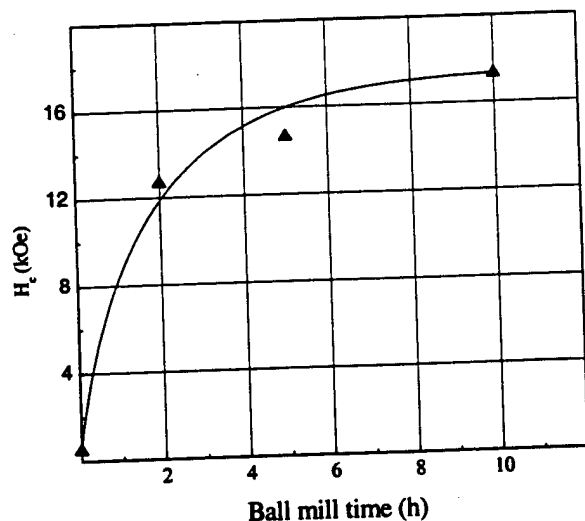


FIG. 5. Coercivity as a function of ball-milling time of the LTP MnBi.

of ball milling. Longer milling time increases the coercivity further but at a slower rate. The increase in coercivity appears to be nearly complete after 10 h of ball milling, which may indicate that the particles are approaching the single domain size.⁷

Figure 6 shows the temperature dependence of coercivity of the LTP of MnBi for samples ball milled at various time periods. For each sample, the coercivity increases with temperature, reaches a maximum at around 300 °C, and then drops rapidly as the temperature increases further. The coercivity is nearly zero at around 350–360 °C due to the LTP-HTP transition. It may be interesting to note that as the ball-milling time increases, the peak in the coercivity versus temperature curve becomes more pronounced. In the LTP of MnBi, the increase in coercivity with the increase in temperature is due to the increase in anisotropy energy.³ It was shown from magnetization measurements made on the LTP of single

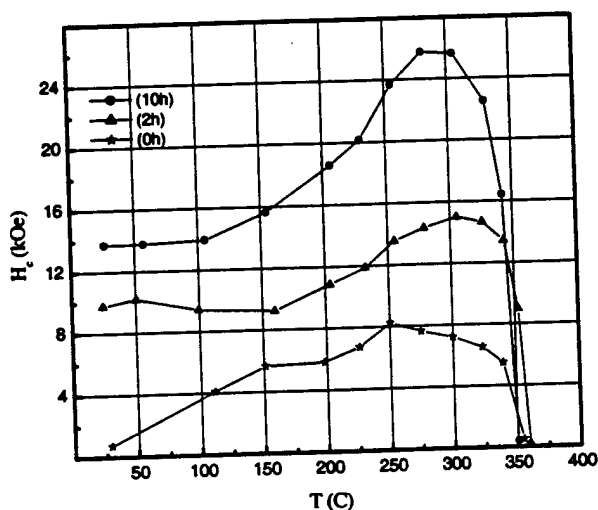


FIG. 6. Temperature-dependent coercivity of LTP MnBi particles obtained after different ball-milling time.

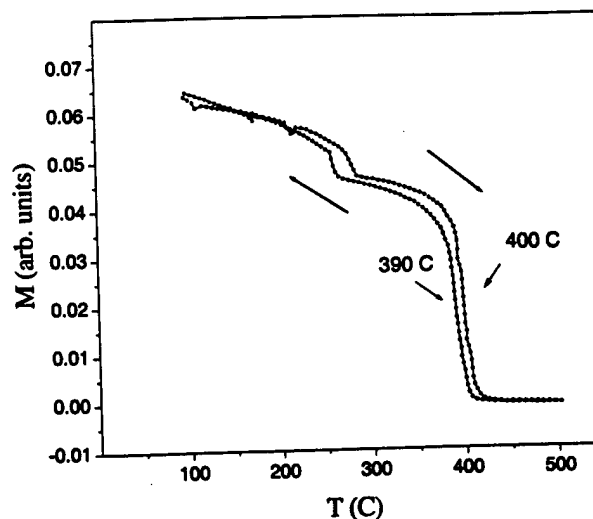


FIG. 7. Magnetization as a function of temperature in an applied field of 500 Oe for $\text{Mn}_{0.75}\text{Ni}_{0.25}\text{Bi}_{0.5}\text{Sb}_{0.5}$.

crystal MnBi that the anisotropy energy increases with temperature and reaches a maximum at 317 °C and then drops at higher temperatures.^{3,6,8} This variation in the coercivity versus temperature behavior observed by us is very similar to the temperature dependence of anisotropy energy reported by Albert and Carr⁶ and by Guo *et al.*⁹

The temperature dependence of magnetization of the $\text{Mn}_{0.75}\text{Ni}_{0.25}\text{Bi}_{0.5}\text{Sb}_{0.5}$ sample is shown in Fig. 7. The magnetic transition is found to be elevated to 400 °C compared to 360 °C in MnBi (both samples were prepared by induction melting). The M - H data (at room temperature) on $\text{Mn}_{0.75}\text{Ni}_{0.25}\text{Bi}_{0.5}\text{Sb}_{0.5}$ indicates that the maximum magnetization (at 1.75 T) increases substantially to 38.8 emu/g compared to about 22 emu/g in MnBi prepared under similar conditions. The substitution possibly prevents segregation of Mn and thus results in the formation of a larger concentration of the magnetic phase. Studies of structural and magnetic properties of $\text{Mn}_{0.75}\text{Ni}_{0.25}\text{Bi}_{0.5}\text{Sb}_{0.5}$ and other variations of this composition are in progress.

ACKNOWLEDGMENTS

This work was supported by DARPA through the Office of Naval Research under Contract No. N14-98-C-0268 and by the Pennsylvania Department of Environmental Protection under Grant No. 97-116.

- ¹X. Guo, A. Zaluska, Z. Altounian, and J. O. Strom-Olsen, *J. Mater. Res.* **5**, 2646 (1990).
- ²C. Guillaud, *J. Phys. Radium* **12**, 492 (1951).
- ³T. Chen and W. Stutius, *IEEE Trans. Magn.* **MAG-10**, 581 (1974).
- ⁴M. Kishimoto and K. Wakai, *Jpn. J. Appl. Phys.* **14**, 893 (1975).
- ⁵X. Guo, A. Zaluska, Z. Altounian, and J. O. Strom-Olsen, *J. Appl. Phys.* **69**, 6067 (1991).
- ⁶P. A. Albert and W. J. Carr, *J. Appl. Phys.* **32**, 201S (1961).
- ⁷S. Saha, M. Q. Huang, C. J. Thong, B. J. Zande, V. K. Chandhok, S. Simizu, R. T. Obermyer, and S. G. Sankar, *J. Appl. Phys.* **87**, 6040 (2000).
- ⁸W. K. Unger, E. Wolfgang, H. Harms, and H. Haudek, *J. Appl. Phys.* **43**, 2875 (1972).
- ⁹X. Guo, X. Chen, Z. Altounian, and J. O. Strom-Olsen, *J. Appl. Phys.* **73**, 6275 (1993).

Structure and magnetic properties of $\text{RCo}_{7-x}\text{Zr}_x$ ($\text{R}=\text{Y, Gd, Nd, or Ho}$, $x=0-0.8$)

M. Q. Huang^{a)} and S. G. Sankar
Advanced Materials Corporation, 700 Technology Drive, P.O. Box 2950, Pittsburgh, Pennsylvania 15230

W. E. Wallace and M. E. McHenry
Carnegie Mellon University, MSE Department, Pittsburgh, Pennsylvania 15213

Q. Chen and B. M. Ma
Rhodia Inc., Rare Earth and Gallium, CN 7500, Cranbury, New Jersey 08512

Alloys with the composition $\text{RCo}_{7-x}\text{Zr}_x$ ($\text{R}=\text{Y, Gd, Nd, or Ho}$, $x=0-0.8$) were synthesized and characterized in the temperature range from 10 to 1273 K and in fields up to 5 T. As with the $\text{R}=\text{Sm, Pr, or Er}$ systems studied earlier in our laboratory, the effects of Zr doping on the stability of TbCu_7 structure phase and changes in the magnetocrystalline anisotropy H_A are observed in the systems in which the rare earth is Y, Gd, Nd, or Ho. Nearly single phase TbCu_7 structure materials were formed in the as-cast alloys when $x=0.1$ and 0.2 . In the case of $\text{R}=\text{Y or Gd}$, a large increase in H_A (which is mainly contributed by Co sublattice) by Zr doping was observed. For $\text{R}=\text{Y}$, H_A increases from 18 kOe for $x=0$ to 74 kOe for $x=0.2$ at 300 K and from 20 kOe for $x=0$ to 82 kOe for $x=0.2$ at 10 K. For $\text{R}=\text{Gd}$, H_A increases from 35 kOe for $x=0$ to 140 kOe for $x=0.2$ at 300 K and to 182 kOe for $x=0.2$ at 10 K. In the case of $\text{R}=\text{Ho and Nd}$, the R-sublattice favors a planar anisotropy at room temperature, presumably due to the negative second order Stevens' coefficient. For $\text{R}=\text{Ho}$, the anisotropy changes from planar for $x=0$ to axial with $H_A \sim 60-70$ kOe at 300 K when $x=0.1$ and 0.2 . For $\text{R}=\text{Nd}$, H_A is dominated by R sublattice which results in a planar anisotropy. Other magnetic properties such as magnetization, Curie temperature, and spin reorientation temperature for these alloys are presented. © 2000 American Institute of Physics. [S0021-8979(00)21508-9]

INTRODUCTION

Currently there is an intense search to find new magnetic materials or to improve existing magnets, particularly for temperature applications. Commercial $\text{Sm}_2\text{Co}_{17}$ -type magnets have compositions close to 1:7. Further, zirconium doping in these magnets improves the permanent magnet properties. A systematic study of the structure and magnetic properties of SmCo_7 -based alloys has been carried out by several groups.¹⁻⁶ Our previous work^{4,6} on the $\text{RCo}_{7-x}\text{Zr}_x$ ($\text{R}=\text{Sm, Pr, or Er}$) systems indicated that partly replacing dumbbells by Zr atoms resulted in stabilizing the TbCu_7 structure and significantly increases the anisotropy. The earlier work has been extended in the present study to include Y (nonmagnetic), Gd (spin only), Nd (light R), or Ho (heavy R).

EXPERIMENTS

The alloys were prepared by arc-melting under argon atmosphere. X-ray diffraction (XRD) with Cu radiation and thermomagnetic analysis (TMA) were used to determine the crystal structure and phases present. Magnetic properties were measured in the temperature range of 10–1273 K and field up to 5 T by using a vibrating sample magnetometer and a superconducting quantum interference device magnetometer. The measured samples were in the forms of chunks, fine random powder, or aligned ($\leq 38 \mu\text{m}$) powder. The

anisotropy field (H_A) was determined by measuring the easy and hard axis magnetization on powder aligned in a field of 1.6 T and fixed in epoxy.

III. RESULTS AND DISCUSSION

A. Structure and phases present of as-cast alloys

Information concerning the structure and the phases present is obtained by XRD and TMA measurement and is given in Fig. 1 and Tables I.

The XRD patterns of the random and aligned powder samples show that the crystal structures of the as-cast alloys $\text{RCo}_{7-x}\text{Zr}_x$ vary significantly with the Zr content x .

For $\text{R}=\text{Nd}$ typical superlattice lines for the $\text{Th}_2\text{Zn}_{17}$ structure, viz., (015) and (204) vanish when $x \geq 0.2$ [See Fig. 1(d)]. This indicates that the structure of the main phase changes from rhombohedral ($\text{Th}_2\text{Zn}_{17}$ type) ($x=0$) to disordered hexagonal (TbCu_7 type) ($x \geq 0.2$). Nearly single phase materials in the TbCu_7 structure were formed for Nd alloys when $x=0.2$. For the aligned samples, XRD indicates that all alloys show planar anisotropy. In the case of $\text{R}=\text{Y, Gd, and Ho}$, the structure of the main phase changes from ordered hexagonal ($\text{Th}_2\text{Ni}_{17}$ type) ($x=0$) to disordered hexagonal (TbCu_7 type)⁵ when $x \geq 0.1$. As shown in Figs. 1(a), 1(b), and 1(c) for the randomly oriented samples, a typical superlattice line, (203), for the $\text{Th}_2\text{Ni}_{17}$ structure disappears when $x \geq 0.1$. For the aligned samples ($\text{R}=\text{Y, Gd}$), two pairs of strong lines at $x=0$, which belong to the 2-17 and 1-7 phases, becomes one pair when $x \geq 0.1$, which belongs to the 1-7 phase. For aligned samples ($\text{R}=\text{Ho}$) a strong uniaxial

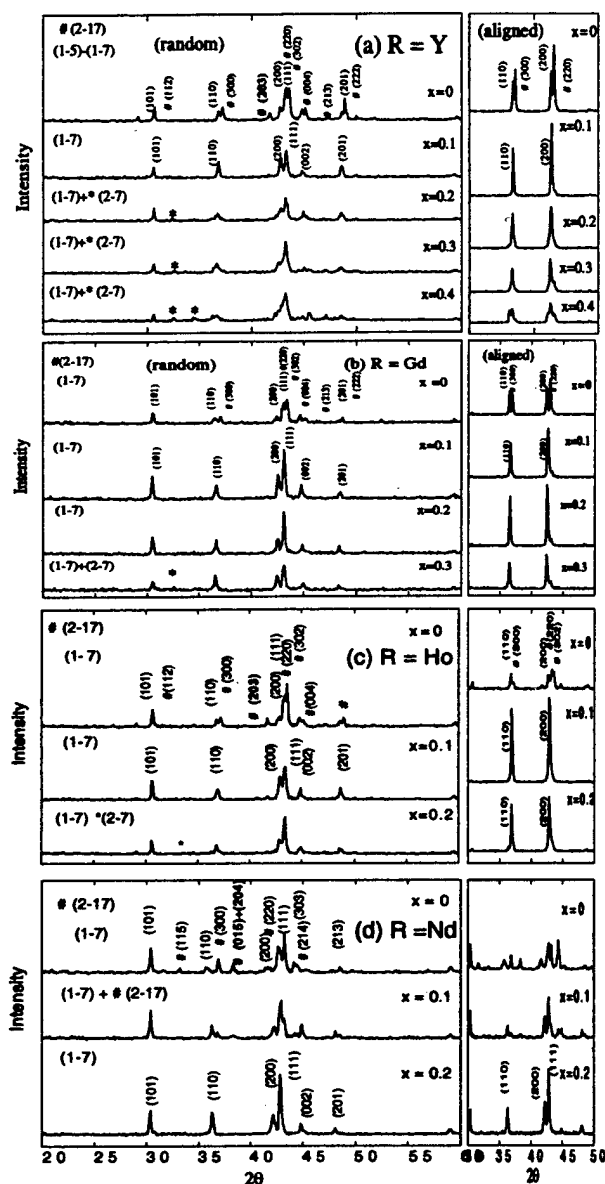


FIG. 1. XRD of $\text{RCo}_{7-x}\text{Zr}_x$ as-cast alloys in random and aligned powder (a) $\text{R}=\text{Y}$, (b) $\text{R}=\text{Gd}$, (c) $\text{R}=\text{Ho}$, and (d) $\text{R}=\text{Nd}$.

anisotropy was detected for $x \geq 0.1$. A nearly single phase material with TbCu_7 structure was formed for $\text{R}=\text{Y}$, Gd , Ho alloys when $x=0.1$. Zr doping can significantly increase the stability of the TbCu_7 structure phase in the RCo_7 alloys. The lattice parameters a and c slightly change as Zr content increases. It can be ascribed to a substitution of Zr for Co dumbbells. As the Zr content was further increased, some other rare earth-rich phases, such as 2-7 (Ce_2Ni_7 or Er_2Co_7 -type), form. The earlier phases were also detected by the TMA measurement (see Table I). The three Curie temperatures (T_{C1} , T_{C2} , and T_{C3}) correspond to the three types of magnetic phases, viz., 2:17, 1:7, and 2:7. We observed a phase transformation from the disordered 1-7 phase to the ordered 2-17 and 1-5 phases at about 750–800 °C in Y, Gd, Nd, or Ho alloys. This was confirmed by XRD measurements in our work. Similar phase transformations were earlier reported^{4,6} in $(\text{Sm}, \text{Pr}, \text{Er})\text{Co}_{7-x}\text{Zr}_x$ alloys.

B. Magnetic properties of as-cast alloys

Variation of Curie temperature of $\text{RCo}_{7-x}\text{Zr}_x$ for alloy examined in this study are given in Table I. As mentioned earlier, for $x=0$ two types of magnetic phases were observed viz., T_{C1} for 2-17 phase and T_{C2} for 1-7 phase. As Zr content increases, amount of the 1-7 phase increases and 2-17 phase decreases. A single magnetic phase 1-7 was formed for $\text{R}=\text{Nd}$ when $x=0.2-0.3$ and for $\text{R}=\text{Y}$, Gd , and Ho when $x=0.1-0.2$. The Curie temperatures are in the range of 730–880 °C, which are around ~ 50 °C lower than that of 2:17 phase and ~ 50 °C higher than that of 1:5 phase. With increase in the Zr content, the T_{C2} for the 1-7 phase slightly decreases. The Curie temperature of $\text{RCo}_{7-x}\text{Zr}_x$ alloys are a measure of the strength of the magnetic interaction which are mainly dominated by Co-Co and to a lesser degree by R-Co and R-R interactions. A dependence of the T_C on the root of the de Gennes function, $(g-1)^2 J(J+1)$ is found for $\text{RCo}_{7-x}\text{Zr}_x$ alloys and is very similar to that of RCo_5 alloys. For $x > 0.3-0.4$, another magnetic phase (2-7 phase with T_{C3}) was also detected.

As shown in Table I and Fig. 2, the anisotropy fields H_A , at both 300 and 10 K were significantly improved by a small amount of Zr substitution. For $\text{R}=\text{Y}$, Gd the anisotropy arises mainly from the 3d, (Co) sublattice, because Y is nonmagnetic and Gd^{+3} has S ground state with zero orbital moment. A large improvement in H_A with Zr doping was observed in these two systems. For Y alloys, H_A increases from 18 kOe for $x=0$ to 74 kOe for $x=0.2$ at 300 K and from 20 kOe for $x=0$ to 82 kOe for $x=0.2$ at 10 K. For Gd alloys, the largest increase in H_A was observed. H_A increases from 35 kOe for $x=0$ to 140 kOe for $x=0.2$ at 300 K, and from basal plane for $x=0$ changes to uniaxial with $H_A \sim 182$ kOe for $x=0.2$ at 10 K. For alloys $\text{R}=\text{Nd}$, H_A is dominated by R-sublattice's planar anisotropy. For alloys with $\text{R}=\text{Ho}$, it is interesting to note that H_A changes from planar for $x=0$ to over 60–70 kOe when $x=0.1-0.2$ at 300 K and to 40 kOe at 10 K (Fig. 2). A spin reorientation occurs at ~ 200 K (Fig. 3).

From the earlier information, we note that a strong uniaxial anisotropy was developed by a small amount of Zr substitution for Co in the earlier $\text{RCo}_{7-x}\text{Zr}_x$ systems. As we pointed out before^{4,5} it can be inferred that replacing the Co dumbbells by Zr atoms can restore the anisotropy of the Co (2c sites) sublattice, which was reduced when Co was replaced by R atoms (i.e., as the $\text{Th}_2\text{Zn}_{17}$ or $\text{Th}_2\text{Ni}_{17}$ structures

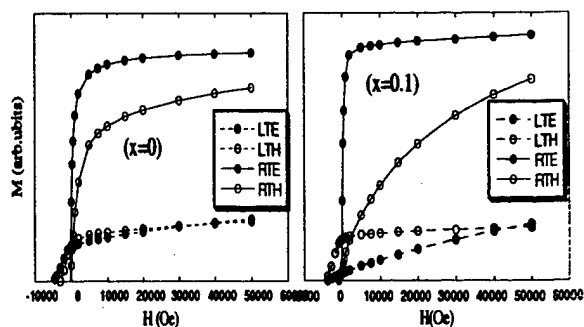


FIG. 2. M vs H of $\text{HoCo}_{7-x}\text{Zr}_x$ as-cast alloys (at 300 and 10 K).

TABLE I. Magnetic properties of $\text{RCo}_{7-x}\text{Zr}_x$ as-cast alloys ($\text{R}=\text{Y}, \text{Gd}, \text{Ho}, \text{or Nd}$) ($x=0-0.8$).^a

R	x	T_C (°C)			M (300 K) (emu/g)	M (10 K) (emu/g)	M (10 K) (μ_B /f.u.)	H_A (kOe)-DoM ^c	
		T_{C1}	T_{C2}	T_{C3}				300 K	10 K
Y	0	894	850		125.1	128.1	11.2	18	20
	0.1		841		114.9	116.6	10.5	50	60
	0.2	(b)	780	414	109.3	112.5	10.3	74	82
	0.3		730	375	117.7	116.2		74	85
	0.4		720	375	90.9	93.6		75	85
	0.8			367	37.3	53.5		75	105
Gd	0	928	879		54.3	44.1	4.5	35	EB
	0.1	b	872		49.7	40.9	4.2	113	148
	0.2	b	840		46.6	35.3	3.6	140	182
	0.5		766	437	30.4	19.6		162	190
	0.8				67.7	21.2	2.19	EB	EB
Ho	0	901	870		68.9	13.2	1.37	65	40 ^d
	0.1		851		61.4	19.9		72	40 ^d
	0.2		813	403	129.0	142.3	14.2	EB	EB
Nd	0	886	729		125.6	133.0	13.3	EB	EC&EB
	0.1		715		121.7	131.2	13.3	EB	EC&EB
	0.2		710						

^a $M(\text{Nd}^{+3}) \sim 3 \mu_B$, $M(\text{Ho}^{+3}) \sim 9 \mu_B$. For Ho alloys $T_{sr} \sim 200$ K, $T_{comp} \sim (50-60)$ K.

^bRelated to (2:17) phase, which was formed after heating up to 750–800° C due to a phase transformation from 1:7 to 2:17 and 1:5.

^cDoM: Direction of magnetization; EB: Easy plane; EC: Easy conical; EA: Easy uniaxial.

^dDoM changes to hard direction at 10 K.

were formed from the CaCu_5 type structure). For $\text{R}=\text{Nd}$ or Ho , H_A also was contributed by the R sublattice. When $x \geq 0.3-0.4$, some other R-rich phases were formed.

The moment M measured at 10 K in a field up to 5 T and in a loose powder form ($\leq 38 \mu\text{m}$) is listed in Table I. As in other R-3d systems, the magnetization in the $\text{RCo}_{7-x}\text{Zr}_x$ systems is contributed from both R^{+3} ion and 3d (Co) ion. From the experimental moment of the $\text{YCo}_{7-x}\text{Zr}_x$ ($x=0-0.1$ and 0.2), we can estimate the moment for Co atom. It decreases slightly from ~ 1.6 to $1.5 \mu_B$, which is nearly the same as that in YCo_5 and Y_2Co_{17} . It was found that the experimental moments for $\text{R}=\text{Nd}$, Ho , or Gd alloys ($x=0-0.1-0.2$) also obey the general rule for the 4f-3d exchange interaction. The light R couple ferromagnetically with Co, while the

heavy R couple antiparallel, which results in a very low saturation for the high-moment heavy rare earth ion. For example, as shown in Fig. 3 in the Ho alloys, the partial moment cancellation resulting from this antiparallel coupling was observed around 50–60 K. The estimated moments for R^{+3} ion in $\text{RCo}_{7-x}\text{Zr}_x$ systems are similar to those in RCO_5 and R_2Co_{17} . For example, $M(\text{Nd})$ is $3.0 \mu_B$ and $M(\text{Ho})$ is $\sim 9.0 \mu_B$, which are very close to their free ion values.

ACKNOWLEDGMENTS

Work carried out at Advanced Materials Corporation was supported by DARPA through the Office of Naval Research under Contract No. N14-98-C-0268. Work carried out at Carnegie Mellon University was supported by AFOSR under Grant No. F49620-96-C-0454.

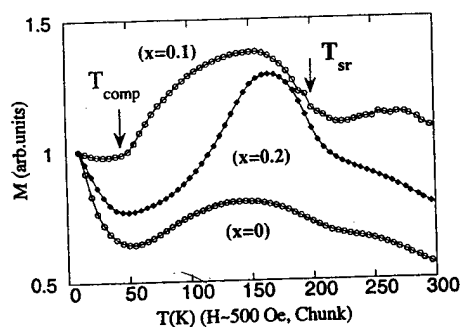


FIG. 3. M vs T of $\text{HoCo}_{7-x}\text{Zr}_x$ as-cast alloys ($H \sim 500$ Oe). T_{sr} : Spin reorientation temperature and T_{comp} : compensation temperature.

- ¹H. Saito, M. Takahashi, T. Wakiyama, G. Kodo, and H. Nakagawa, J. Magn. Magn. Mater. **82**, 322 (1989).
- ²K. H. J. Buschow and F. J. A. den Broeder, J. Less-Common Met. **3**, 191 (1973).
- ³J. Yang, O. Mao, and Z. Altounian, IEEE Trans. Magn. **23**, 2702 (1987).
- ⁴M. Q. Huang, W. E. Wallace, M. McHenry, Q. Chen, and B. M. Ma, J. Appl. Phys. **83**, 6718 (1998).
- ⁵Y. Khan, Acta Crystallogr., Sect. B: Struct. Crystallogr. Cryst. Chem. **29**, 2502 (1973).
- ⁶M. Q. Huang, M. Drennan, W. E. Wallace, M. McHenry, Q. Chen, and B. M. Ma, J. Appl. Phys. **85**, 5663 (1999).